Journal of Asian Concrete Federation

journal homepage: https://jacf.sfulib3.publicknowledgeproject.org/index.php/jacf

γ-C_2S-Based Binders for Low-Carbon Concrete: Carbonation and Performance

Ziyi Tang[1], Hengji Zhang[2*], Xufei Liu[3], Hui Li[1*], Fazal Rehman[1], Liyang Wang[1], Jingbin Yang[1]

[1] *Key Laboratory of Road and Traffic Engineering of the Ministry of Education, College of Transportation Engineering, Tongji University, Shanghai 201804, China*
[2] *STHG Technology Transformation Co.,Ltd, Taiyuan, Shanxi-030000,PR China*
[3] *Department of Structural Engineering, Jacobs School of Engineering, University of California, San Diego, La Jolla, CA 92093-0085, USA*

A B S T R A C T

Gamma-dicalcium silicate (γ-C_2S) is a nonhydraulic clinker phase that can harden through carbonation, linking cement reduction with CO_2 mineralization. Existing reviews mainly address carbonatable binders broadly or individual modification strategies. Here, γ-C_2S is examined across formation, carbonation, structure, performance, and scale-up. Recent studies found that carbonation degree alone does not govern performance. A multiphase clinker containing 51 wt.% γ-C_2S reached 83.8% carbonation and 93 MPa compressive strength after 24 h, while an aragonite-rich product assemblage increased compressive strength by 57.3% and reduced porosity by 29.2% relative to a calcite-dominated reference. However, scale-up introduces a competing limitation: increasing specimen thickness from 0.5 to 4 in. reduced CO_2 uptake from 26.6% to 4.3%. These results shift the design target from maximizing phase purity, CO_2 pressure, or carbonation degree toward controlling phase assemblage, moisture–gas accessibility, and product organization. Controlled multiphase binders and thin, nonreinforced precast products therefore appear most realistic for near-term deployment, while durability, reinforcement compatibility, process energy, and net-carbon accounting remain key challenges.

Keywords: γ-Dicalcium silicate (γ-C_2S); Carbonation hardening; CO_2 mineralization; Carbonatable binders; Microstructural evolution

1.Introduction

Decarbonizing cement and concrete requires not only reducing clinker-related emissions but also developing material routes that can permanently mineralize CO_2 during manufacture and curing. Because a substantial fraction of cement-sector emissions originates from limestone decarbonation, energy substitution alone cannot eliminate process emissions. Recent low-carbon strategies therefore increasingly combine clinker reduction, alternative binder chemistry, and CO_2 utilization [1,2]. Among these approaches, carbonatable binders are distinctive because CO_2 is not merely stored passively but participates directly in hardening through the precipitation of stable carbonate phases [3,4]. Recent assessments further indicate that carbonatable binders can complement conventional low-clinker systems, particularly in factory-controlled products where carbonation conditions and component geometry can be regulated [5].

Gamma-dicalcium silicate (γ-C_2S) represents a particularly unusual member of this binder family. Conventionally regarded as an undesirable, nearly nonhydraulic C_2S polymorph, γ-C_2S undergoes transformation-induced self-pulverization during clinker cooling but becomes highly reactive when moisture and CO_2 are simultaneously available. Carbonation releases Ca^{2+} from the silicate lattice, precipitates $CaCO_3$, and leaves a progressively polymerized silica-rich phase; the resulting crystalline–amorphous product network fills pores and connects initially weak particle contacts. Recent studies further show that the engineering response cannot be inferred from γ-C_2S content or carbonation degree alone. Industrial-grade and multiphase γ-C_2S clinkers can exhibit reaction and strength characteristics different from those of high-purity laboratory material, while γ-C_2S may achieve a higher carbonation degree than β-C_2S without developing the higher mechanical strength [6–8]. Thus, the central issue is not simply whether γ-C_2S carbonates, but how mineral composition, reaction pathway, and product organization convert CO_2 uptake into a mechanically effective structure.

*Corresponding author: Hengji Zhang (hengjizhang@126.com), Hui Li (hli@tongji.edu.cn)

DOI http://dx.doi.org/10.18702/acf.2026.12.1.???

Received: 24-Jun-2026; Revised: 19-Aug-2026; Accepted: 03-Sep-2026; Published online: 17-November-2026

ISSN 2465-7964, eISSN 2465-7972. Copyright © Asian Concrete Federation, All rights reserved.

Recent research has consequently shifted from maximizing carbonation rate toward controlling the coupled reaction–transport process. Moisture regulates the competition between mineral dissolution, ionic transport, and CO_2 access, so both insufficient and excessive water can suppress effective mineralization [9–11]. Product accumulation further creates surface-to-core gradients and progressively changes the rate-controlling step, making carbonation uniformity increasingly important as specimen dimensions increase [12]. Strategies developed in the past few years therefore target different parts of this coupled process: multiphase clinker design adjusts the reactive phase assemblage [13], internal carbonation supplies inorganic carbon to poorly carbonated interior regions [14], and ion or additive regulation modifies dissolution and carbonate precipitation [15]. At the same time, recent corrosion evidence shows that the low alkalinity produced by extensive carbonation creates a service-performance constraint that is fundamentally different from that of conventional Portland cement systems [16]. These developments indicate that the practical viability of γ-C_2S depends on coordinating reaction kinetics, product structure, transport uniformity, durability, and manufacturing conditions rather than optimizing any single carbonation parameter.

Existing reviews have established the general chemistry and classification of nonhydraulic calcium-silicate and carbonatable binders [3,4,17], while more recent work has specifically summarized ion-doping effects in γ-C_2S, C_3S_2, and CS systems [15]. However, a γ-C_2S-centered synthesis linking clinker formation and compositional control to interfacial carbonation, product evolution, transport-controlled hardening, engineering performance, and scale-up remains lacking. Accordingly, this review examines γ-C_2S-based binders across the complete production–carbonation–structure–performance–application chain. Particular attention is given to the distinction between high-purity laboratory γ-C_2S and industrial multiphase feedstocks, the coupling between reaction and mass transport, the roles of $CaCO_3$ polymorphism and silica-gel polymerization, and the implications of these processes for mechanical performance, durability, CO_2 accounting, and engineering deployment. This framework is intended to clarify both the opportunities and the practical limits of γ-C_2S as a scalable carbonatable binder.

2. Formation and Characteristics of γ-C_2S

2.1 Crystal Structure and Polymorphic Transformation

Dicalcium silicate (Ca_2SiO_4) occurs mainly as the α, d H, α′ L, β, and γ polymorphs. The high-temperature α and α ′ forms transform progressively during cooling, while monoclinic β-C_2S can persist metastably and orthorhombic γ-C_2S is thermodynamically stable under ambient conditions [18]. The β-to-γ transformation involves changes in Ca coordination and rotation of the SiO_4 tetrahedra and is accompanied by an approximately 12% increase in lattice volume, leading to cracking and clinker self-pulverization. The extent of β-C_2S retained at room temperature is therefore controlled by factors including grain size, cooling history, synthesis conditions, and foreign ions [19]. The olivine-like structure of γ-C_2S consists of isolated SiO_4 tetrahedra linked through Ca–O polyhedra, which contributes to its very low hydraulic reactivity. Recent electronic-structure and enhanced-sampling calculations show that the γ-C_2S (010) surface exhibits lower initial hydration reactivity than β-C_2S, reflecting differences in Ca coordination, oxygen electron density, and surface Ca-dissolution pathways [20]. This structural stability does not imply chemical inertness: under humid CO_2 exposure, interfacial water facilitates H_2O dissociation and Ca dissolution, while dissolved CO_2-derived species promote progressive decalcification and carbonate formation [21]. γ-C_2S therefore behaves as a carbonation-activated rather than a conventional hydraulic phase, with its reactivity strongly dependent on the interfacial chemical environment.

As summarized in Fig. 1, the β-to-γ transformation gives γ-C_2S clinker a distinctive self-pulverizing behavior. Transformation-induced volume expansion promotes spontaneous disintegration, thereby reducing the subsequent crushing and grinding demand [6]. In practical multiphase clinkers, however, the extent of γ-C_2S formation and self-pulverization is coupled to the overall phase assemblage and raw-material composition, which also influences the subsequent carbonation response [22]. Self-pulverization is therefore not only a processing advantage but also an important link between clinker formation and later carbonation performance.

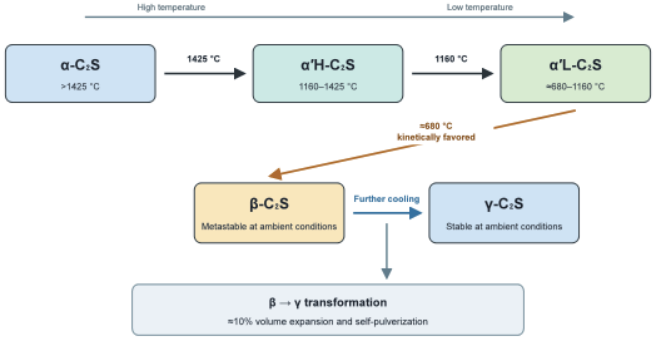


Fig 1 Schematic transformation sequence of the principal C_2S polymorphs during cooling.

2.2 Formation Routes and Compositional Effects

High-temperature solid-state reaction followed by controlled cooling is the conventional route for synthesizing γ-C_2S. Laboratory preparation typically uses $CaCO_3$ or CaO with SiO_2 at a Ca/Si molar ratio close to 2.0. The mixed precursors are generally fired at approximately 1350–1450 ° C and subsequently cooled to promote γ-C_2S formation [18,23]. This route provides good control over composition and phase assemblage and is therefore well suited to mechanistic studies. However, reagent-grade precursors and prolonged high-temperature treatment increase both cost and energy demand, limiting its suitability

for large-scale production.

Natural mineral feedstocks can improve the industrial feasibility of γ-C_2S production while maintaining a relatively high γ-C_2S content. Huang et al. [6] prepared industrial-grade γ-C_2S clinker from limestone and sandstone using an optimized mass ratio of 2.1 and a firing temperature of 1400°C. The resulting clinker was dominated by γ-C_2S and retained the characteristic self-pulverization behavior during cooling. Compared with reagent-derived γ-C_2S, the industrial-grade material exhibited a more complex particle morphology and a more moderate carbonation rate, which helped limit rapid moisture loss and improved post-carbonation strength. These results demonstrate that low-cost mineral resources can produce reactive γ-C_2S while reducing dependence on high-purity laboratory precursors.

Ion regulation provides an additional means of controlling both clinker formation and subsequent carbonation. Liu et al. [24] showed that Na, P, and K suppressed the β-to-γ transformation, whereas Mg, Ti, Ni, and Cu had relatively limited effects on the final polymorphic composition but altered particle size and surface morphology. At the crystal-chemical level, impurity-induced stabilization occurs when foreign ions are incorporated into the C_2S lattice and preferentially stabilize a particular polymorph. Substitution at Ca^{2+} or Si^{4+} sites can introduce local lattice distortion and, for aliovalent dopants, charge-compensating defects, thereby modifying the coordination environment and relative stability of the C_2S polymorphs. Preferential stabilization of β-C_2S can consequently delay or suppress its transformation to γ-C_2S during cooling, allowing the metastable β phase to persist over a lower-temperature range.

Phosphorus provides a representative example of this mechanism. PO_4^{3-} units can substitute for SiO_4^{4-} in the C_2S lattice, with the resulting charge imbalance compensated by Ca vacancies, thereby stabilizing β- and α-C_2S at room temperature [25]. Further electronic-structure analysis showed that P incorporation induces lattice distortion and shifts the electronic energies of Ca, Si, and O toward lower-energy states. Accordingly, 0.6 wt.% P_2O_5 increased the β-C_2S fraction by 50.8 wt.% in an AOD-slag system [26]. A similar β-phase stabilization has recently been reported for V^{5+} incorporation, whereas excessive V addition promotes $Ca_2V_2O_7$ formation and limits its incorporation into the C_2S structure [27]. The possible substitution sites of foreign ions in γ-C_2S and their effects on carbonation reactivity are illustrated in Fig. 2.

Other dopants act mainly through morphology and carbonation reactivity rather than phase stabilization. Mg, Ti, Ni, and Cu can reduce particle size and increase surface folding, thereby changing the effective reaction area [24]. Ti addition, for example, increased the carbonation degree and compressive strength by 15.6% and 75.7%, respectively, whereas Zn had an adverse effect. These contrasting behaviors indicate that impurity effects depend not only on dopant concentration but also on whether the foreign species preferentially regulate polymorphic stability or modify the morphology and reactivity of the resulting γ-C_2S.

At industrial scale, γ-C_2S clinker is generally multiphase rather than phase-pure. Depending on the feedstock and clinker chemistry, γ-C_2S may coexist with β-C_2S, calcium aluminosilicates, free CaO, and amorphous phases. These associated phases can alter phase transformation, self-pulverization, carbonation kinetics, and interparticle bonding [7]. Multiphase clinkers may therefore achieve performance comparable to high-purity γ-C_2S even at lower γ-C_2S contents, provided that the associated phases and interfaces are favorable. Industrial clinker design should consequently target a controlled phase assemblage rather than maximum γ-C_2S purity alone. Representative formation routes are compared in Table 1 using available quantitative data on γ-C_2S content, carbonation conditions, carbonation degree, and compressive-strength response.

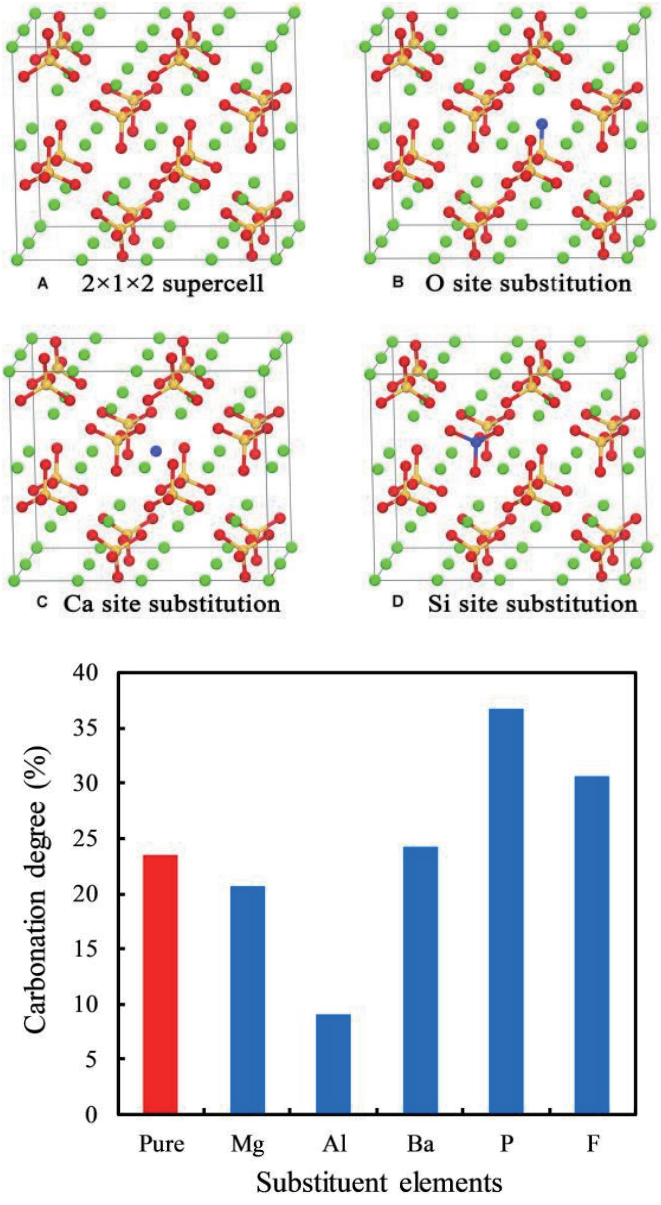


Fig 2 Possible substitution sites of foreign ions in γ-Ca_2SiO_4 and their effects on carbonation reactivity. [28]

Table 1. Representative γ-C_2S formation routes and quantitative carbonation performance

Formation route	Raw materials / synthesis conditions	γ-C_2S content (wt.%)	Carbonation conditions	Carbonation degree (%)	Compressive strength (MPa/ relative change)	Ref.
Multiphase clinker production	AR $CaCO_3$ + SiO_2 + Al_2O_3; 1400 ° C, 3 h; $\gamma_{51}G_{42}$ clinker	51	99% CO_2, 0.3 MPa; w/b = 0.15; 30 MPa compaction; 24 h	83.8	93	[7]
Reagent-based solid-state synthesis	CaO + SiO_2, molar ratio 2:1; 1350 ° C, 3 h; furnace cooling	92.4	Natural carbonation	—	—	[18]
Natural mineral-based clinkerization	Limestone/ sandstone, mass ratio = 2.1; 1400 ° C, 3 h; natural cooling	63	99.9% CO_2, 0.3 MPa; w/b = 0.15; 30 MPa compaction; 24 h	43.7	48% greater compressive strength tested at 24 h	[6]
Ion-regulated synthesis	$Ca(OH)_2$ + SiO_2, molar ratio 2:1; 3.0 wt.% Ti dopant; 1400 ° C, 3 h	—	99.9% CO_2, 0.3 MPa, RH ⩾ 95%; w/s = 0.15; 30 MPa compaction; 24 h	+15.6*	+75.7*	[24]

Note: For the ion-regulated route, Ti was selected as the representative dopant because it produced the largest improvement among the investigated ions. The reported increases in carbonation degree (+15.6%) and compressive strength (+75.7%) are relative to the undoped pure γ-C_2S control under identical carbonation conditions.

Overall, the difference between high-purity laboratory γ-C_2S and industrial multiphase binders is not simply a matter of phase purity. High-purity γ-C_2S primarily provides a reference for its intrinsic carbonation pathway, whereas industrial clinkers behave as coupled phase assemblages in which secondary phases, impurity chemistry, and particle characteristics jointly redistribute reaction kinetics and product formation. A lower γ-C_2S content can therefore still produce equal or better mechanical performance when the overall phase assemblage moderates premature surface reaction, preserves internal moisture, promotes carbonate nucleation, or improves interparticle bonding. Industrial clinker design should therefore focus on how the phase assemblage organizes carbonation and load transfer rather than on maximizing γ-C_2S purity alone.

2.3 Hydration and Carbonation Reactivity

γ-C_2S exhibits negligible hydraulic hardening under conventional water curing but develops strength rapidly when moisture and CO_2 are simultaneously available. Guan et al. [29] reported that γ-C_2S mortar failed to harden under water curing, whereas aqueous carbonation produced flexural and compressive strengths of 10.10 and 61.82 MPa, respectively, within 24 h. This contrast identifies γ-C_2S as a carbonation-activated rather than a conventional hydraulic binder: water provides the medium for CO_2 dissolution and ionic transport, while dissolved CO_2 promotes mineral dissolution and decalcification.

Reaction extent alone, however, does not determine mechanical performance. Under identical carbonation conditions, Du et al. [30] found that γ-C_2S exhibited the highest carbonation degree but the lowest compressive strength among α′ L-, β-, and γ-C_2S. Zhao et al. [31] further showed that strength depends on solid-volume change, $CaCO_3$ morphology and distribution, and interparticle bonding in addition to the extent of reaction. CO_2 uptake should therefore be evaluated together with the efficiency with which carbonation products develop a continuous load-bearing structure.

The carbonation of γ-C_2S is fundamentally a structural reorganization process driven by Ca^{2+} leaching, calcium carbonate precipitation, and polymerization of the residual silica-rich phase. Its idealized reaction can be expressed as follows in equation 1:

$$Ca_2SiO_4 + 2CO_2 + nH_2O \rightarrow 2CaCO_3 + SiO_2{\cdot}nH_2O \quad (1)$$

Complete decalcification gives γ-C_2S a theoretical CO_2-binding capacity of approximately 51.1% of its initial mass, although practical uptake is lower because of moisture and transport limitations and progressive product-layer formation. The resulting $CaCO_3$ and silica-rich phases fill pores and connect neighboring particles, while their spatial distribution determines how effectively reaction products contribute to hardening [24]. The carbonated fracture surface in Fig. 3 illustrates this heterogeneous product-filled microstructure together with residual C_2S.

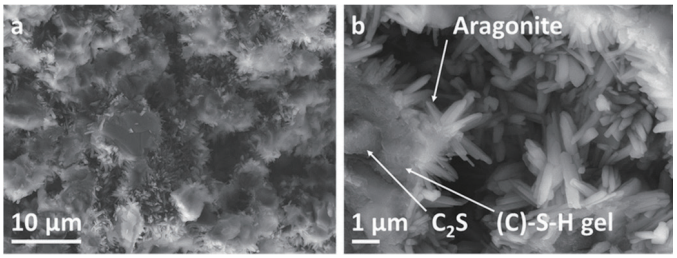


Fig 3 SEM analysis of fracture surface carbonated γ-C_2S: (a) a magnification 2,500 × (b) magnification 10,000 ×. [11]

Fig 4 presents the X-ray diffraction (XRD) pattern of the tested material. The diffraction peaks indicate the presence of two crystalline phases, γ-C_2S (▲) and β-C_2S (★). The strong γ-C_2S peaks, particularly around 30° , 33° , and 48° (2θ), suggest that γ-C_2S is the dominant crystalline phase, while the β-C_2S peaks appear at several lower-intensity positions. Overall, the pattern confirms the coexistence of both C_2S polymorphs in the material.

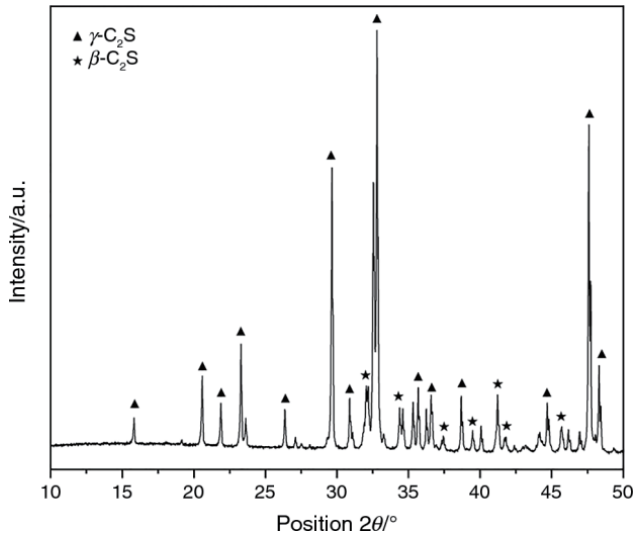


Fig 4 X-ray diffraction pattern of the as-synthesized material, in which γ-C_2S is the dominant phase and β-C_2S occurs as a minor phase.[11]

3. Carbonation Mechanisms

3.1 CO_2 Dissolution and Interfacial Decalcification

The preceding discussion establishes that carbonation activates γ-C_2S, but reaction extent alone does not determine the resulting mechanical performance. Understanding this decoupling requires examining the coupled dissolution, transport, and precipitation processes initiated at the γ-C_2S–CO_2 interface.

Carbonation of γ-C_2S is a coupled gas–liquid–solid process involving CO_2 transport, aqueous speciation, and mineral dissolution. Gaseous CO_2 penetrates connected pores and dissolves in the interfacial water film, establishing equilibria among H_2CO_3, HCO_3^-, and CO_3^{2-}. The equilibria among these species can be simplified as follows in equations 2, 3, 4, and 5:

$$CO_2(g) \rightleftharpoons CO_2(aq) \quad (2)$$

$$CO_2(aq) + H_2O \rightleftharpoons H_2CO_3 \quad (3)$$

$$H_2CO_3 \rightleftharpoons H^+ + HCO_3^- \quad (4)$$

$$HCO_3^- \rightleftharpoons H^+ + CO_3^{2-} \quad (5)$$

The resulting acidification promotes Ca release from the γ-C_2S surface, while interfacial water simultaneously provides the medium for dissolved-carbon transport and participates directly in surface reactions. Recent ab initio calculations identified both dry and water-assisted carbonation pathways on the γ-C_2S (010) surface. In the water-assisted pathway, unsaturated lattice oxygen facilitates H_2O dissociation, while water coordinated to surface Ca promotes Ca dissolution; the resulting hydroxyl species subsequently react with CO_2 to form HCO_3^- and, ultimately, carbonate species [21] . Thus, interfacial water is not merely a solvent for CO_2 but an active component of the carbonation reaction. The reactivity of the interface is further controlled by the local atomic structure. Oxygen vacancies introduce localized charge states that enhance CO_2 activation, facilitate dynamic Ca^{2+} leaching, and lower the kinetic barrier for carbonate formation [32]. These findings indicate that interfacial decalcification is governed not only by solution chemistry but also by the electronic and defect structure of the γ-C_2S surface.

Progressive Ca^{2+} release produces a decalcified, Si–OH-rich surface layer and can be represented ideally as follows:

$$Ca_2SiO_4 + 4H^+ \rightarrow 2Ca^{2+} + H_4SiO_4 \quad (6)$$

Continued Ca leaching progressively destabilizes the original Q^0 silicate framework and provides the precursor for subsequent silicate condensation and polymerization, as discussed in Section 3.2. Recent enhanced-sampling calculations further show that modification of the surface electronic structure can shift the competition between direct surface carbonation and dissolution–precipitation: Fe incorporation promotes water hydroxylation and Ca^{2+} dissolution while suppressing the kinetically limited direct surface route, thereby favoring deeper carbonation through dissolution and precipitation [33].

Taken together, these studies support a predominantly water-assisted dissolution–transport–precipitation mechanism under practical humid curing conditions, although direct surface carbonation may coexist locally.

3.2 Formation and Evolution of Carbonation Products

The principal products of γ-C_2S carbonation are $CaCO_3$ polymorphs and silica-rich gel. Calcium released into the pore solution combines with CO_3^{2-} and precipitates as calcium carbonate according to the following reaction in equation 7:

$$Ca^{2+} + CO_3^{2-} \rightarrow CaCO_3 \quad (7)$$

At the same time, the silicate species remaining after calcium leaching undergo condensation and form a highly polymerized amorphous phase [34,35]. This silica-rich phase generally retains a limited amount of calcium and is therefore more accurately described as Ca-modified silica gel rather than

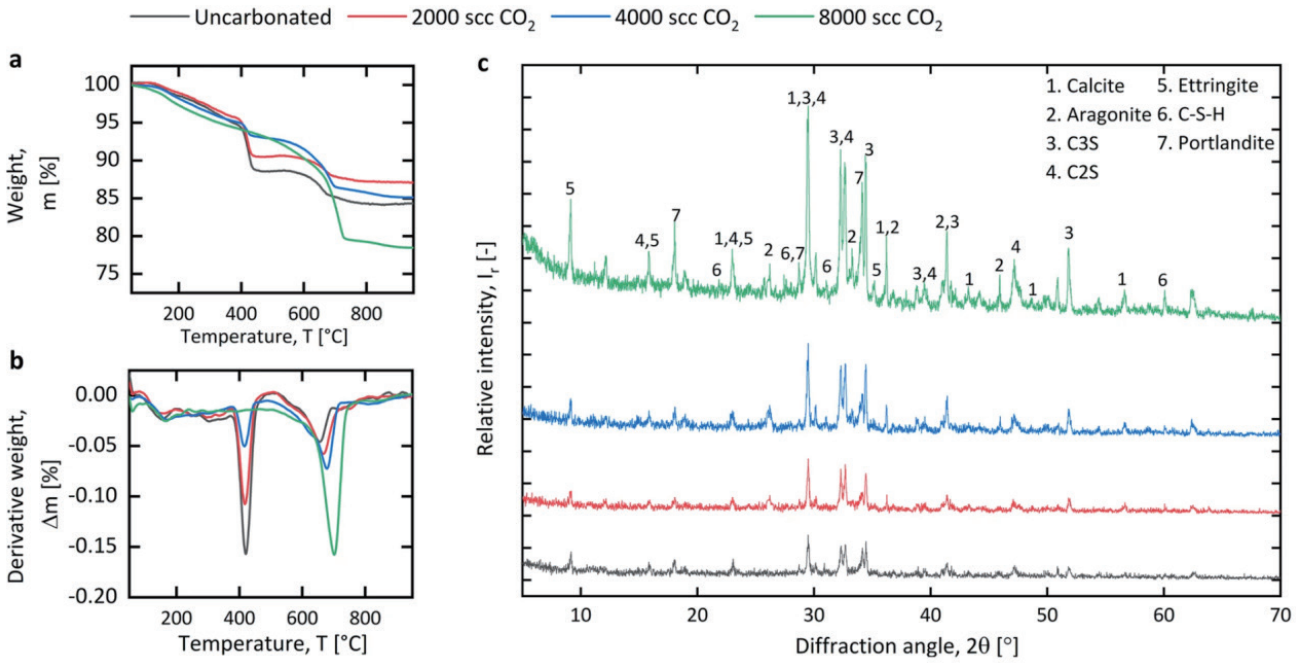


Fig 5 Characterization of carbonated and uncarbonated cement suspensions. TGA curves of cement suspensions. b DTA curves of cement suspensions. c XRD spectra of carbonated and uncarbonated cement suspensions.[39]

completely calcium-free SiO_2 gel. $CaCO_3$ provides volumetric filling and a crystalline skeleton, whereas the silica-rich gel forms continuous connections between particles and carbonate crystals. The coupled formation of these two product groups consequently provides the material basis for carbonation-induced hardening.

$CaCO_3$ generally evolves from initially metastable products toward more stable crystalline forms during carbonation. During early carbonation, high ionic supersaturation favors the rapid nucleation of amorphous calcium carbonate and fine vaterite crystals, whereas aragonite and calcite gradually form as the reaction proceeds [34,35]. The resulting phase assemblage is governed by the local reaction environment, including pH, Ca^{2+}/CO_3^{2-} ratio, moisture state, and CO_2 availability [36–38]. The influence of carbon supply on carbonate evolution is illustrated in Fig. 5: increasing CO_2 flow alters the extent of carbonate formation and produces the coexistence of calcite and aragonite within the reacting calcium-silicate matrix [39]. These observations indicate that $CaCO_3$ formation should be understood as a condition-dependent phase-evolution process rather than the formation of a single stable carbonate product.

Carbonate precipitation is accompanied by progressive reorganization of the decalcified silicate phase. As γ-C_2S becomes decalcified, condensation between silicate tetrahedra creates Si–O–Si bonds and converts the residual amorphous phase from a weakly polymerized structure into a more continuous three-dimensional network [34,35]. The resulting silica-rich gel can occupy the spaces between unreacted γ-C_2S and $CaCO_3$ crystals, thereby contributing to interparticle bonding. Its effect is nevertheless spatially dependent: a continuous and well-connected gel phase strengthens the product network, whereas excessive accumulation around residual particles can hinder Ca^{2+} release and CO_2 transport. Silica-rich gel therefore acts simultaneously as a binding phase and as a potential transport barrier during later carbonation.

Quantitative phase and spectroscopic data further show that carbonation-product evolution cannot be described by carbonation degree alone (Table 2). Even at comparable reaction levels, γ-C_2S systems can develop markedly different $CaCO_3$ assemblages, while the residual silicate phase evolves from Q^0-rich environments toward highly polymerized Q^3–Q^4-rich gel. These differences directly affect how the carbonated matrix is constructed. For example, increasing the in-situ aragonite content to approximately 67% was accompanied by increases of 64.9% and 57.3% in flexural and compressive strength, respectively, together with a 29.2% reduction in total porosity and a decrease in the most probable pore size from 1.34 to 0.67 μm relative to a calcite-dominated reference. This demonstrates that carbonate polymorphism strongly influences pore filling, crystal bridging, and load transfer.

Silicate polymerization contributes through a different structural pathway. The shift toward Q^3–Q^4-rich configurations reflects the development of a more connected silica-rich network, which improves continuity across unreacted particles and carbonate crystals. The performance of carbonated γ-C_2S therefore emerges from the coordinated evolution of carbonate crystal morphology and silicate-network connectivity: the former reorganizes pore space and mechanical interlocking, whereas the latter strengthens interfacial continuity within the product network.

3.3 Multistage Reaction Kinetics and Transport Control

The carbonation of γ-C_2S generally consists of an early rapid-reaction stage followed by a slower diffusion-controlled

Table 2. Representative quantitative data for $CaCO_3$ polymorphism and silicate polymerization during γ-C_2S carbonation

Carbonation condition	Quantitative $CaCO_3$ characteristics	Silicate polymerization	Ref.
99.9% CO_2, 0.2 MPa, w/s = 0.15, 2 h	$CaCO_3$ = 45.0 wt.%; mainly calcite with minor vaterite	Q^0 53.9%, Q^3 10.2%, Q^4 35.9%	[40]
100% CO_2, WCT = 0.730 μm, 48 h	Outer layer: 23.6% aragonite, 30.1% calcite; inner layer: 57.7% aragonite, 13.4% calcite	—	[41]
TEA-regulated carbonation, 7 d	Aragonite = 62–67% for TEA γ-C_2S = 0.005–0.009	—	[42]
>99% CO_2, 0.30 MPa, 24 h; 2 mol/L NH_4Cl	Predominantly calcite-containing products	$Q^0/Q^3/Q^4$ = 25.25/27.95/46.80%, Q^4/Q^3 = 1.67; NH_4Cl:11.84/43.42/44.74%, Q^4/Q^3 = 1.03	[43]
Aqueous carbonation, 10% CO_2, ~20 ° C, 6 h	$CaCO_3$ = 73.6 wt.%; calcite dominant	Q^3/Q^4 = 0.64; Q^4-dominated silica gel	[44]
Comparable carbonation degree; 20% CO_2, 20 ° C, 99% RH	Type C: 57% calcite; Type A: 69% aragonite; Type V: 67% vaterite	—	[45]

Note: Q^n denotes SiO_4 tetrahedra containing n bridging oxygen atoms. WCT denotes water coating thickness. The percentages reported by different studies are not directly interchangeable because the quantification bases differ, including QXRD phase fractions, carbonate mass fractions, and ^{29}Si NMR relative Si-site populations.

stage. Ashraf and Olek [23] analyzed the carbonation of different calcium silicate phases using a contracting-volume model and the Jander diffusion equation. They found that the early stage was mainly governed by chemical reactions at the phase boundary, whereas the later stage gradually became controlled by diffusion through the product layer. Initially, CO_2 can readily reach γ-C_2S surfaces through open pores, allowing Ca^{2+} leaching and $CaCO_3$ nucleation to occur simultaneously. Carbonation heat release, mass gain, and strength development are therefore rapid during this period. As the reaction proceeds, the products cover the particle surfaces and fill the surrounding pores, increasing the transport distance between the unreacted core and external CO_2. The kinetics of γ-C_2S carbonation thus progressively shift from phase-boundary control to product-layer diffusion control.

As carbonation proceeds, $CaCO_3$ and silica-rich products progressively fill pores and coat unreacted particle surfaces, narrowing transport pathways and increasing the distance between external CO_2 and the reaction front [35]. CO_2 must then diffuse inward through gas-filled pores, water films, and the product layer, while dissolved Ca^{2+} migrates outward. Excessive surface precipitation may therefore create a dense carbonated shell around an incompletely reacted core. Product densification is thus beneficial to early strength development but can progressively restrict further carbonation. This transport-controlled spatial heterogeneity is also observed in other carbonatable calcium-silicate systems. As illustrated in Fig. 6, the cross-sectional distribution of calcite in carbonated rankinite varies markedly with curing duration and temperature, reflecting the changing balance between reaction rate and CO_2 transport. Although rankinite is not γ-C_2S, this profile provides a useful analogue for understanding how transport limitations can generate nonuniform carbonation fronts in γ-C_2S-based materials.

The dynamic evolution of pore-solution pH controls the balance between γ-C_2S dissolution and $CaCO_3$ precipitation. A relatively low pH increases proton attack on Ca–O bonds and promotes Ca^{2+} leaching, whereas a higher pH increases the proportion of CO_3^{2-} among dissolved inorganic carbon species and strengthens the driving force for $CaCO_3$ precipitation [36,38]. As CO_2 continues to dissolve, OH^- is consumed and the pore-solution pH decreases, causing the dominant inorganic carbon species to shift from CO_3^{2-} toward HCO_3^- and H_2CO_3. Excessively low or high local pH conditions may therefore disrupt the balance between dissolution and precipitation. Sustained carbonation requires these two processes to remain kinetically compatible so that the reaction front can advance into the particle interior. Accordingly, pH is not an isolated reaction parameter but a central chemical variable connecting CO_2 dissolution, γ-C_2S decalcification, and $CaCO_3$ nucleation.

Soluble carbonate salts further reveal the importance of aqueous inorganic carbon supply in γ-C_2S carbonation. Zhou et al. [36] used a saturated NH_4HCO_3 solution as the carbonation medium and achieved substantial γ-C_2S reaction

under atmospheric pressure. Unlike gaseous curing, which relies on the dissolution of externally supplied CO_2, NH_4HCO_3 directly provides HCO_3^- in the aqueous phase. This approach reduces the limitation imposed by gas–liquid mass transfer while promoting Ca^{2+} leaching and $CaCO_3$ precipitation. The results indicate that improving carbonation efficiency does not necessarily require a substantial increase in gaseous CO_2 pressure. Instead, maintaining sufficient dissolved inorganic carbon and effective ionic transport at the particle surface may be equally important. The supply and speciation of aqueous inorganic carbon are therefore fundamental to understanding the carbonation kinetics of γ-C_2S.

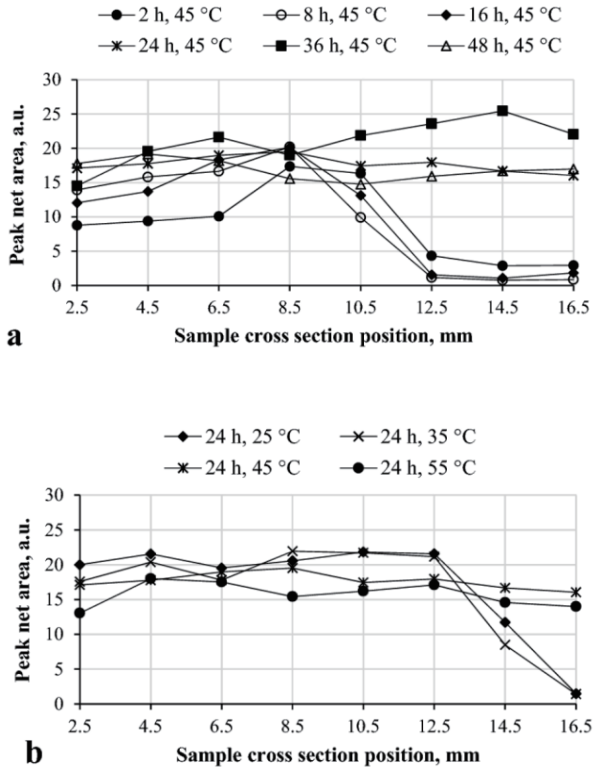


Fig. 6. Cross-sectional distribution of the calcite XRD peak area in carbonated rankinite as a function of curing duration (a) and temperature (b). [46]

3.4 Carbonation-Induced Hardening and Hydration–Carbonation Coupling

Carbonation-induced hardening of γ-C_2S arises primarily from precipitation-induced pore filling and interparticle bonding. $CaCO_3$ crystals and silica-rich gel progressively occupy capillary pores and bridge adjacent particles, transforming the initially compacted powder into a continuous load-bearing matrix [34,35]. The resulting strength, however, depends not only on the amount of carbonation products but also on their morphology, spatial distribution, and interfacial compatibility. Effective hardening therefore requires the formation of well-connected reaction products at mechanically favorable locations rather than simple pore filling alone.

The sequence of hydration and carbonation can alter both the reaction pathway and the hardened structure of γ-C_2S. Luo et al. [47] found that γ-C_2S remained a loose powder after hydration alone but became substantially densified after subsequent carbonation as $CaCO_3$ precipitated within the pore network. Repeated carbonation–hydration cycles could further activate residual C_2S, although newly formed hydration products could also modify local porosity and transport pathways. This path dependence is illustrated schematically in Fig. 7 using a Ca-silicate-rich ladle-furnace slag system, where hydration products and residual C_2S/C_3S are progressively transformed during carbonation into $CaCO_3$ and a Ca-deficient gel. Although the system is not pure γ-C_2S, it captures the same mechanistic principle relevant here: products formed during one stage modify the phases, interfaces, and transport conditions available for the next. Hydration and carbonation should therefore be regarded as coupled, sequence-dependent processes rather than independent reactions.

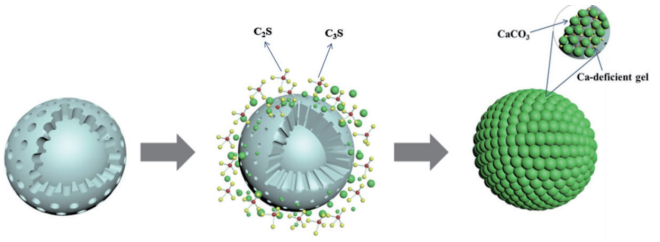


Fig 7 Schematic hydration–carbonation coupling in Ca-silicate-rich ladle-furnace slag, illustrating the transformation of hydrated and residual silicate phases into $CaCO_3$ and Ca-deficient gel during subsequent carbonation. [48]

Overall, γ-C_2S carbonation comprises a sequence of coupled processes, including CO_2 transport and dissolution, carbonic acid adsorption, Ca–O bond cleavage, Ca^{2+} leaching, $CaCO_3$ nucleation and growth, and silica-rich gel polymerization. The early reaction is dominated by surface chemistry and phase-boundary advancement, whereas the later stage gradually becomes diffusion controlled as $CaCO_3$ and silica-rich gel form a denser product layer. The resulting performance depends on the reaction extent, $CaCO_3$ polymorphism, gel polymerization, and spatial distribution of the products rather than on any single factor. Carbonation of γ-C_2S should therefore be understood as a multistage process involving continuous feedback among chemical reactions, ionic transport, and microstructural evolution.

4. Factors Governing Carbonation

The carbonation of γ-C_2S is governed by the combined effects of external CO_2 supply, aqueous reaction conditions, pore transport, and solid-phase reactivity. CO_2 must first penetrate the pore network and dissolve in the water films surrounding the particles. The resulting dissolved inorganic carbon species then react with Ca^{2+} released from γ-C_2S. Consequently, increasing the CO_2 concentration, water content, or compaction pressure does not necessarily produce a continuous improvement, because enhancing one process may restrict another. For example, elevated CO_2 pressure

can accelerate early carbonation but may also promote rapid surface precipitation, thereby limiting subsequent gas transport. Therefore, the carbonation conditions of γ-C_2S should be optimized by balancing reaction kinetics with mass transport.

4.1 CO_2 Concentration, Pressure, and Curing Duration

CO_2 concentration and partial pressure primarily determine the driving force for early γ-C_2S carbonation. Increasing the CO_2 partial pressure generally enhances the gas supply at the gas–liquid interface and accelerates Ca^{2+} release and $CaCO_3$ precipitation, leading to faster early strength development. In an MgO–γ-C_2S system, Zhang et al. [49] found that carbonate formation and strength development proceeded substantially faster under 100% CO_2 than under 10% CO_2. Nevertheless, the strength achieved after 8 h at 10% CO_2 was comparable to that obtained after 4 h at 100% CO_2. This result indicates that the effect of a lower CO_2 concentration can be compensated for by extending the curing period, highlighting the potential for directly using low-concentration industrial flue gas. Overall, increasing the CO_2 concentration mainly reduces the time required to reach a target degree of carbonation rather than independently determining the final performance.

Curing duration controls the transition of γ-C_2S carbonation from an interface-controlled reaction to a diffusion-controlled process. Zhao et al. [50] divided extended carbonation into three stages: phase-boundary reaction control, CO_2 diffusion through the product layer, and combined control by CO_2 diffusion and Ca^{2+} dissolution. At the beginning of carbonation, the exposed γ-C_2S surface dissolves rapidly, followed by the precipitation of carbonation products. As $CaCO_3$ and silica gel progressively accumulate around the particles, the product layer becomes denser and the subsequent reaction rate decreases. A comparative study of calcium silicates similarly showed that the degree of carbonation and strength of γ-C_2S increased rapidly during the early period, whereas the additional benefits of prolonged curing gradually diminished [51]. Therefore, continuously extending carbonation under a constant high CO_2 concentration or pressure may offer limited benefits, while staged regulation of pressure and curing time may improve overall efficiency.

4.2 Temperature and Moisture State

Temperature controls carbonation by simultaneously affecting chemical kinetics, ionic transport, CO_2 solubility, and $CaCO_3$ polymorphism. An increase in temperature generally accelerates γ-C_2S dissolution and $CaCO_3$ nucleation, thereby promoting early carbonation. However, elevated temperatures also reduce the solubility of CO_2 in pore water and accelerate moisture loss from the specimen. Lu et al. [52] demonstrated that increasing the curing temperature from 5 to 50 ° C accelerated carbonation and early strength development in CO_2-cured cement paste. Temperature also significantly altered the relative proportions, morphologies, and crystallinity of calcite, aragonite, and vaterite. Although their study was not conducted on pure γ-C_2S, the competition among dissolution, diffusion, and precipitation identified in that work is also applicable to carbonation-hardening calcium silicate systems. Temperature therefore affects carbonation not only through reaction kinetics and CO_2 solubility but also by modifying the interfacial moisture environment. As shown in Fig. 8, increasing temperature changes both the thickness and density distribution of adsorbed water films at silicate surfaces. Such changes directly influence the continuity of the aqueous layer available for Ca^{2+} transport and CO_2 speciation, thereby coupling thermal effects with moisture-controlled reaction and mass transfer.

An appropriate moisture state is essential for γ-C_2S dissolution and CO_2 ionization, whereas excessive water restricts the penetration of gaseous CO_2. When the water content is insufficient, continuous water films cannot form on particle surfaces, limiting Ca^{2+} transport and the conversion of dissolved CO_2 into HCO_3^- and CO_3^{2-}. Conversely, excess water fills the available pores, and CO_2 transport through the liquid phase is considerably slower than through the gas phase. Chen et al. showed that particle packing density and water film thickness explain variations in the degree of carbonation and strength more directly than the conventional water-to-solid ratio. Zhang et al. [23] further reported that a degree of carbonation of at least 45% was most readily achieved when the void fraction ranged from 18% to 28% and the water volume fraction ranged from 22% to 27%. Moreover, the appropriate water volume fraction increased with the void fraction. Therefore, moisture optimization essentially requires a balance between the water films needed for ionic reactions and the gas-filled pathways needed for CO_2 transport.

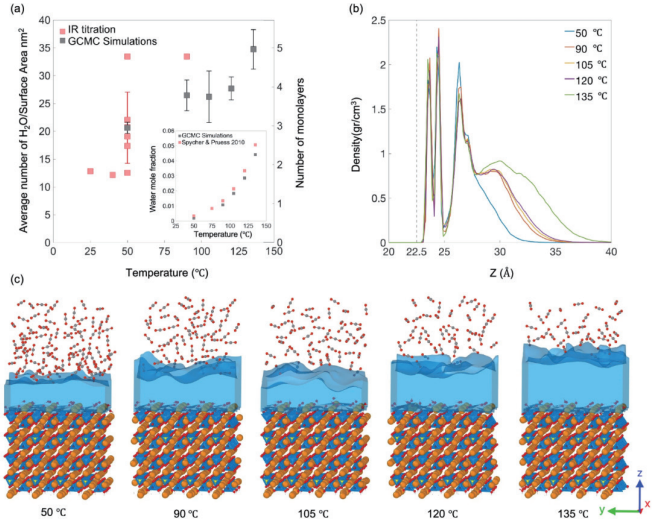


Fig 8 Temperature-dependent evolution of interfacial water nanofilms during silicate carbonation: (a) simulated and experimentally measured water-film thickness, (b) water-density profiles normal to the mineral surface, and (c) molecular configurations showing the increase in adsorbed water layers with temperature. The results were obtained for hydroxylated forsterite and are presented as mechanistic evidence for water-film-mediated carbonation. [23]

4.3 Particle Packing and Pore Structure

Particle packing controls γ-C_2S carbonation by simultaneously regulating reactive surface area, interparticle contact, water-film distribution, and gas-accessible pore space. Finer particles provide more reactive surface, but excessive fines increase water demand and may restrict connected CO_2-transport pathways. Similarly, dense packing strengthens the initial compact but can limit gas penetration. Chen et al. [41] showed that particle packing and water-film thickness describe the resulting carbonation and strength response more directly than the nominal water-to-solid ratio. Particle-size design should therefore balance surface reactivity with the accessibility of both water and CO_2 rather than simply maximizing fineness or packing density.

The same trade-off extends to the pore network: excessive densification promotes surface-localized carbonation, whereas excessive porosity weakens the load-bearing framework even when the reaction degree is high [23] . The resulting strength is therefore highly sensitive to how the initial pore structure is established during processing. As illustrated in Fig. 9, variations in binder content and forming load markedly change the compressive strength of a carbonation-hardened wollastonite–larnite system, while extending CO_2 curing produces progressively smaller strength gains. These trends emphasize that compaction, pore accessibility, and curing duration must be coordinated rather than optimized independently. Porous mineral modification further illustrates this principle: replacing 30 wt.% of γ-C_2S with coral powder increased the compressive strength from 79.1 to 88.5 MPa, whereas the same replacement level of quartz powder reduced it to 52.8 MPa [53]. The improvement was attributed to internal transport pathways together with aragonite-assisted $CaCO_3$ nucleation. An effective pore structure should therefore preserve connected CO_2 pathways while enabling carbonation products to form mechanically continuous interparticle bonds.

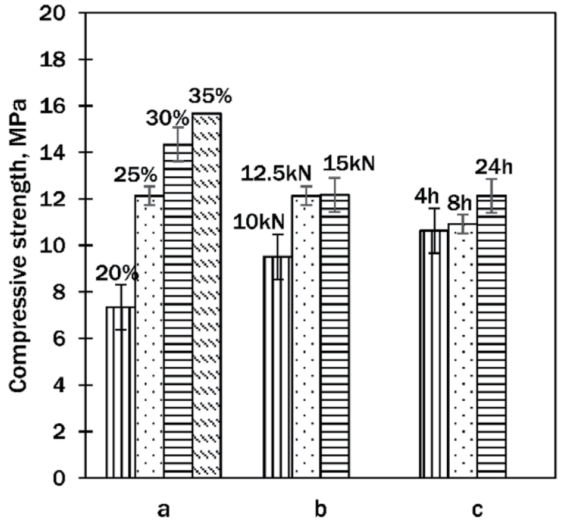


Fig 9 Representative effects of material dosage and processing conditions on the compressive strength of a carbonation-hardened wollastonite–larnite binder: (a) binder content, (b) forming load, and (c) CO_2-curing duration. [54]

The importance of this moisture–pore balance increases with specimen size. In small or thin specimens, CO_2 can access a large fraction of the internal pore network before extensive product accumulation restricts transport. As the diffusion distance increases, however, moisture and gas accessibility become progressively heterogeneous through the specimen depth. Near-surface regions carbonate and densify first, reducing connected gas-filled pathways, whereas the interior can retain more moisture and remain less accessible to gaseous CO_2. Carbonation uniformity therefore depends on maintaining sufficient interfacial water for dissolution and ionic transport while preserving a connected gas-accessible pore network throughout the section. For larger components, bulk carbonation degree alone may consequently obscure surface-to-core differences, and should be complemented by spatial measurements of moisture state, carbonation products, and mechanical response.

4.4 Mineral Composition and Modifiers

Mineralogical regulation provides a direct means of balancing carbonation capacity and mechanical performance. Because β-C_2S and γ-C_2S differ in hydraulic and carbonation reactivity, their proportions determine how rapidly reaction products form and how effectively they contribute to strength. Jiang et al. [55] showed that increasing the γ-C_2S fraction favored carbonation, whereas β-C_2S contributed more strongly to mechanical development; a mixture containing 60% β-C_2S and 40% γ-C_2S reached 54.4 MPa with a carbonation degree of 36.7%. The key design variable is therefore the reactive phase assemblage rather than the γ-C_2S content alone. This broader role of mineralogical engineering is also evident in Fig. 10, where conversion of Mg-silicate resources into akermanite-rich clinkers markedly increased both CO_2 uptake and compressive strength under identical carbonation conditions. Phase design can thus be used to coordinate carbon-mineralization capacity with the formation of a mechanically effective product network.

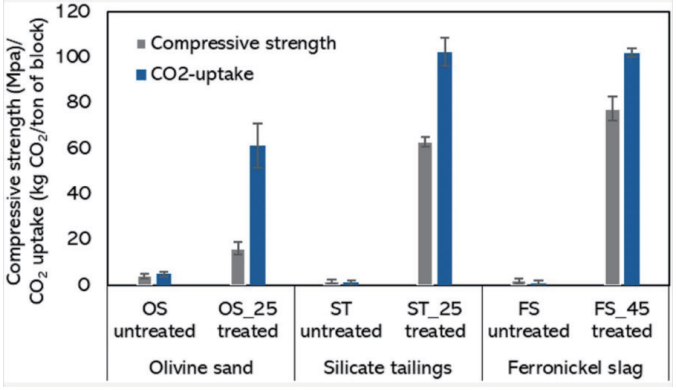


Fig 10 Influence of mineralogical engineering on the compressive strength and CO_2 uptake of carbonation-cured silicate binders. The results compare untreated Mg-silicate resources with their corresponding akermanite-rich clinkers after carbonation at 10 bar and 60 ° C for 16 h. [56]

Ion doping provides a finer level of control by modifying lattice stability, Ca^{2+} release, particle morphology, and carbonate precipitation. Importantly, the most effective dopant is not necessarily the one that produces the fastest initial reaction. Ba incorporation, for example, suppressed early Ca^{2+} release and delayed carbonation, but the slower surface reaction allowed more sustained CO_2 penetration and improved later-age carbonation and strength [57]. This behavior illustrates a broader principle: dopants should be assessed by their effects on reaction depth and product evolution over time rather than by early carbonation rate alone.

Organic additives and surface treatments regulate carbonation mainly at the solid–liquid interface by enhancing Ca^{2+} release, CO_2 dissolution, or $CaCO_3$ nucleation. Chitosan addition increased the compressive and flexural strengths of carbonated γ-C_2S by 66.3% and 298.9%, respectively, through Ca^{2+} coordination and promoted calcite formation [58], while biomineralization pretreatment increased the 30 min compressive strength by 43.66% by providing carbonate nucleation sites [59]. More recently, 1% triethanolamine was shown to enhance both CO_2 dissolution and Ca^{2+} leaching, enabling atmospheric-pressure carbonation to approach the reaction rate achieved under pressurized curing [60]. Excessive addition, however, reduced carbonation, indicating that these strategies are effective only within an appropriate dosage window.

In conclusion, effective modification should accelerate carbonation without sacrificing reaction depth or product-network continuity. Reactivity-enhancing strategies such as Ti doping and low-dose TEA promote γ-C_2S activation and interfacial CO_2/Ca^{2+} transport, whereas Ba modification shows that moderating the initial reaction can sustain deeper carbonation. Organic and biomineralization-assisted additives provide complementary control over carbonate nucleation and interfacial bonding. The key design criterion is therefore to coordinate reaction kinetics, transport depth, and the stability of the resulting carbonate–silica network.

4.5 Integrated Optimization of Carbonation Conditions

The carbonation of γ-C_2S should be optimized through the coordinated design of curing parameters, forming characteristics, and material composition rather than through isolated single-factor adjustments. High CO_2 concentrations may be suitable for shortening the early curing period of precast products, whereas low-concentration CO_2 can be effectively utilized by extending the curing duration or incorporating components that promote Ca^{2+} release. Meanwhile, the water volume fraction and forming pressure should be adjusted according to particle-size distribution to preserve both continuous water films and connected internal gas pathways. Mineral phases and functional modifiers should be selected according to the specific rate-controlling step; porous components can improve transport, seed crystals can promote nucleation, and complexing agents can enhance Ca^{2+} release. Future studies should combine multifactor experiments, coupled reaction–transport modeling, and life-cycle assessment to identify suitable processing windows for different product dimensions and CO_2 sources. Therefore, efficient γ-C_2S carbonation ultimately depends on establishing a dynamic balance among CO_2 supply, ionic reactions, pore transport, and product bonding.

5. Performance Development

The performance development of γ-C_2S materials is fundamentally governed by the interaction among carbonation reactions, product formation, and pore-structure evolution. This hardening pathway distinguishes γ-C_2S from conventional hydraulic binders such as ordinary Portland cement (OPC) and low-clinker systems such as limestone calcined clay cement (LC^3), as well as from chemically activated binders such as alkali-activated materials (AAMs). Whereas hydration or alkali activation can proceed throughout the binder matrix once water or activator is available, γ-C_2S requires a continuous supply of external CO_2 through the connected pore network. Its mechanical strength, dimensional stability, transport resistance, alkalinity, and thermal response are therefore intrinsically coupled to carbonation uniformity as well as to the amount and spatial distribution of the reaction products. Under well-controlled curing, this mechanism enables rapid pore filling, interparticle bonding, and early strength development. However, it also makes performance more sensitive to moisture state, gas-accessible porosity, specimen geometry, and curing conditions. Consequently, the performance of γ-C_2S should be assessed not by carbonation degree or strength alone, but through the coupled relationships among reaction extent, product assemblage, pore structure, spatial uniformity, and service environment.

5.1 Mechanical Strength Development

The mechanical strength of carbonated γ-C_2S originates from the development of a continuous load-bearing network formed by $CaCO_3$ and silica-rich products. As carbonation proceeds, these products fill interparticle pores and strengthen contacts between adjacent γ-C_2S particles, allowing substantial strength to develop within a relatively short curing period [14,61,62] . However, strength is not proportional to carbonation degree alone. Premature surface densification can restrict further CO_2 transport and leave an incompletely reacted core, whereas well-distributed products promote more effective interparticle bonding. Mechanical development therefore depends on both reaction extent and the spatial organization of the carbonation products.

Flexural performance is even more sensitive to product morphology and interfacial continuity. In situ–formed needle- or rod-like aragonite can bridge neighboring particles and pores and thereby improve resistance to crack propagation [42,63]. Interfacial regulation through Mg-containing carbonates or biomimetic molecules can further modify $CaCO_3$ nucleation and improve bonding between carbonate crystals and the silica-rich phase [64]. Conversely, coarse or locally agglomerated crystals and discontinuous silica-rich regions may introduce weak interfaces, so a higher carbonation degree

does not necessarily produce better flexural performance [65]. Thus, flexural strength is governed primarily by crystal morphology, bridging efficiency, and interfacial integrity, rather than by the total amount of $CaCO_3$ alone.

Additional constituents improve strength only when they beneficially modify early-age stability, carbonation transport, or product formation without excessively diluting reactive γ-C_2S. Calcium aluminate cement can stabilize the compact before carbonation, although its prehydration products may alter moisture availability and CO_2 transport, making pre-drying important[61]. Inert fillers can improve packing and provide heterogeneous nucleation sites, whereas excessive replacement reduces the amount of reactive binder [59]. Internal carbonation strategies provide another route by supplying carbonate species to poorly carbonated interior regions and improving reaction uniformity [66,67]. Similarly, limited incorporation of hydraulic constituents can support setting and early strength, but excessive substitution changes the original carbonation-hardening pathway [68,69]. Composite design should therefore balance reactive-phase content, transport accessibility, and early structural stability rather than maximizing any single constituent.

Among low-carbon binder systems, γ-C_2S is distinguished by a carbonation-driven strength-development pathway. LC^3 can maintain mechanical performance comparable to OPC at substantially reduced clinker contents through the synergistic hydration of clinker, calcined clay, and limestone, while appropriately designed alkali-activated materials can also achieve comparable or high mechanical strength through activation of aluminosilicate precursors [70,71]. In γ-C_2S, CO_2 participates directly in matrix formation, converting the initially non-hydraulic particles into a $CaCO_3$–silica-rich product network and enabling substantial strength development within a short curing period [14,61,62]. The coupling of CO_2 mineralization with rapid hardening therefore represents a distinctive mechanical advantage of γ-C_2S. Its realization, however, depends on maintaining sufficient CO_2 transport throughout the reacting matrix, linking mechanical development directly to curing and specimen geometry.

5.2 Microstructural Densification and Pore Evolution

Carbonation-induced pore refinement provides the structural basis for the macroscopic performance of γ-C_2S materials. As carbonation proceeds, $CaCO_3$ and silica-rich products progressively occupy capillary pores and interparticle regions, reducing pore size while strengthening particle contacts [72]. The carbonated matrix is therefore better described as a multiphase network composed of residual silicate particles, silica-rich interfacial regions, and carbonate-filled pores rather than as a uniformly densified solid [73]. $CaCO_3$ contributes rigid filling and mechanical interlocking, whereas the silica-rich phase improves continuity between carbonate crystals and unreacted particles. A representative microstructural arrangement is illustrated in Fig. 11, where residual calcium-silicate phases are surrounded by amorphous silica and $CaCO_3$ after carbonation [74]. This spatial organization helps explain how pore refinement and load transfer develop simultaneously during carbonation hardening.

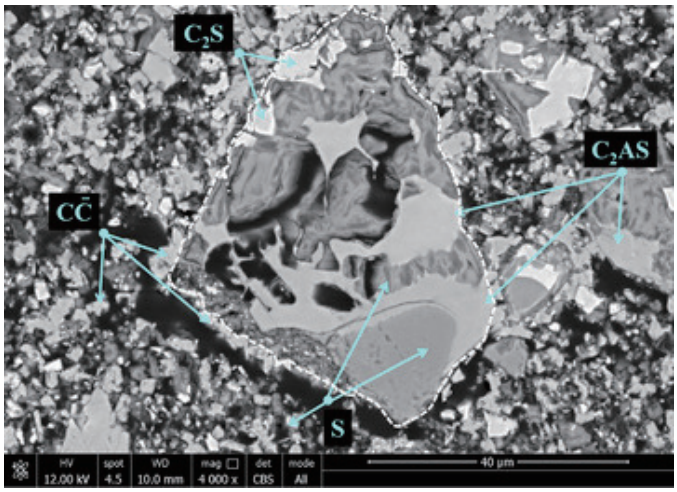


Fig 11 Solidified CS slurry after carbonation with amorphous silica (S), $CaCO_3$ (CC), unreacted gehlenite - åkermanite (C_2AS - C_2MS_2 solid solution) and belite (C_2S). The white dotted line outlines the original form of the uncarbonated CS - particle. Composition of phases given in cement notation. HFW = 103 µm. [74]

Total porosity alone, however, does not adequately describe mechanical performance. Materials with similar porosity can differ substantially in pore-size distribution, connectivity, and interfacial quality. Fine calcite can efficiently fill interparticle voids, whereas high-aspect-ratio aragonite provides a stronger bridging contribution to flexural performance [42,63]. Fine vaterite may also participate in pore filling and mechanical interlocking under suitable conditions [68]. These differences show that pore refinement is governed not simply by the amount of solid products formed, but by how the carbonation products reorganize the pore space and particle contacts. Carbonate morphology primarily determines local filling, interlocking, and bridging, while the silica-rich phase maintains continuity across particle–carbonate interfaces. Their spatial integration therefore determines whether pore refinement is effectively translated into load transfer and mechanical performance.

Excessive surface densification may reduce average porosity while still leaving poorly reacted interior regions and heterogeneous load-bearing paths. Structural optimization should consequently target a spatially continuous and well-bonded multiphase network with controlled pore connectivity, rather than minimum total porosity alone.

5.3 Dimensional Stability, Alkalinity, and Durability

The dimensional stability of carbonated γ-C_2S is governed primarily by spatial moisture gradients generated during carbonation rather than by water content alone. Water is required for CO_2 dissolution and Ca^{2+} transport, while evaporation and carbonation reactions progressively redistribute moisture

within the specimen. Real-time neutron imaging of related carbonation-cured calcium-silicate cement systems has shown that surface drying and internal moisture redistribution directly control the movement of the carbonation front [62]. Internal carbonation can reduce the reaction difference between exterior and interior regions. This effect has been demonstrated directly in γ-C_2S systems [14], while similar internal-carbonate strategies have also been reported for broader calcium-silicate cements [67]. Dimensional stability therefore depends on limiting moisture and reaction gradients that may otherwise generate differential shrinkage, particularly in thicker specimens.

The durability of carbonated γ-C_2S is controlled by a balance between carbonation-induced pore densification and the accompanying reduction in alkalinity. A denser carbonated matrix can restrict the ingress of external ions, but decalcification lowers the pore-solution pH and therefore changes the chemical protection available to embedded steel. This effect has recently been quantified directly in γ-C_2S systems: carbonation reduced the simulated pore-solution pH from approximately 12 to 10 and increased the iron corrosion rate to about 2–4.5 times that under Portland-cement conditions [16] . Direct γ-C_2S studies show that Na_2CO_3 post-curing can partially restore alkalinity while maintaining mechanical performance [66], whereas γ-C_2S-based protective coatings have reduced capillary water absorption by 58% and free and total chloride contents in the underlying concrete by 68% and 60%, respectively [75]. The same coating retained approximately 90% of its bonding strength after 28 d of irradiation, providing direct evidence of short-term durability in a γ-C_2S-based application.

Evidence for salt and sulfate resistance is currently derived mainly from related carbonation-cured calcium-silicate cement systems rather than phase-pure γ-C_2S. Farnam et al. examined carbonated calcium-silicate pastes and mortars saturated with water, NaCl, or $MgCl_2$ solutions under low-temperature freeze–thaw testing and found that the response depended strongly on salt chemistry [76] . More recently, Bersisa et al. exposed carbonated calcium-silicate cement with W/C ratios of 0.35–0.45 to 50 g/L Na_2SO_4 or $MgSO_4$ solutions for 18 months. Na_2SO_4 caused only limited expansion, whereas $MgSO_4$ promoted $CaCO_3$ degradation and critical expansion in the highest-W/C specimens[77] . These studies show that the durability of carbonation-hardened silicate matrices depends not only on pore refinement but also on the chemical stability of the carbonate-containing product network under specific exposure conditions.

Placed in a broader binder context, these results highlight that different low-carbon binders rely on different durability mechanisms. OPC combines a hydration-derived pore structure with a highly alkaline pore solution, whereas LC^3 retains this hydraulic framework while further improving transport resistance through pore refinement and chloride binding. Recent results showed that LC^3 mortar reduced the effective chloride diffusion coefficient by up to 97.6% and increased chloride-binding capacity by up to 38% relative to the Portland-cement reference [78]. Alkali-activated binders can likewise develop low permeability and strong resistance to chloride ingress, freeze–thaw cycling, and other aggressive exposures, although their durability response is more sensitive to precursor composition, activator chemistry, and curing conditions [79].

Carbonated γ-C_2S develops durability through a distinct carbonation-derived protection mechanism. The precipitation of $CaCO_3$ together with silica-rich products progressively disconnects capillary pathways and forms a dense barrier against external species. This effect has been demonstrated directly in γ-C_2S-based protective systems: a carbonated γ-C_2S coating reduced capillary water absorption by 58% and decreased free and total chloride contents in the underlying concrete by 68% and 60%, respectively [75]. The durability advantage therefore lies in coupling CO_2 mineralization with microstructural densification and transport resistance, while long-term performance additionally depends on the chemical stability of the carbonated product network and the control of pore-solution alkalinity when steel reinforcement is involved.

5.4 Thermal Stability

Beyond chemical durability under aqueous and aggressive environments, the stability of the carbonation-derived product network under thermal exposure is also critical to γ-C_2S performance. At low and intermediate temperatures, dehydration and further condensation of the silica-rich phase occur concurrently with thermal deformation of the carbonate-containing matrix [80]. These changes may partly preserve local bonding but also increase porosity and generate thermal mismatch among $CaCO_3$, silica-rich products, and residual γ-C_2S. The resulting microcracking causes a progressive reduction in mechanical performance, with the extent of degradation influenced by the $CaCO_3$ polymorph assemblage and its morphology [81].

More severe deterioration occurs when $CaCO_3$ enters its major decomposition range. CO_2 release disrupts the carbonate-bonding network and generates additional porosity, while the resulting CaO may subsequently rehydrate and induce expansion during cooling or later moisture exposure [80,81]. Thermal performance is therefore governed not simply by the initial degree of carbonation but by the stability of the multiphase product network during heating and cooling. This distinguishes carbonated γ-C_2S from conventional hydration-dominated binders and makes $CaCO_3$ decomposition and post-cooling dimensional stability central considerations for high-temperature applications.

5.5 Functional and Application-Oriented Performance

Beyond conventional mechanical and durability requirements, carbonated γ-C_2S can also serve as a functional matrix when secondary phases are deliberately introduced. Piezoelectric ceramics such as lead zirconate titanate can be incorporated to form 0–3 composites with combined mechanical and electromechanical responses under relatively mild carbonation curing [82]. The functional benefit, however,

depends on maintaining sufficient matrix continuity: increasing the functional-phase content can improve piezoelectric and dielectric properties, whereas excessive addition compromises forming quality and mechanical integrity. Calcium–magnesium carbonation binders have likewise been used to improve compatibility between the functional phase and the surrounding matrix [83]. Figure 12 further shows that compositional modification changes the mass-loss and carbonate-decomposition characteristics after carbonation, indicating that functional design can also alter the phase assemblage and thermal response of the carbonated matrix [84]. Functionalization should therefore be treated as a coupled optimization of functional-phase content, carbonation reaction, and matrix continuity rather than as simple additive incorporation.

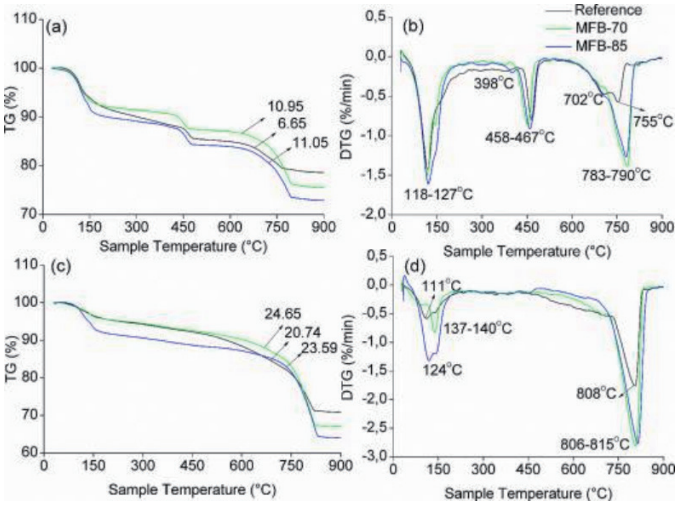


Fig 12 TGA-DTG curves of Reference and MFB with different proportions: (a) TGA and (b) DTG curves of uncarbonated samples and (c) TGA and (d) DTG curves of carbonated samples. [84]

Functional performance can also be created through component-scale architecture. In γ-C_2S-based foamed materials, a highly porous structure lowers thermal conductivity, while carbonation products reinforce the pore walls; one recent study achieved a thermal conductivity of 0.0496 W/(m · K), a compressive strength of 0.5 MPa, and a CO_2 uptake of 45.4% [85]. Additive manufacturing provides a complementary route by increasing exposed surface area and enabling more uniform CO_2 access during forming, thereby improving carbonation and interlayer performance [86]. The performance of these systems is governed by pore architecture, interlayer bonding, and transport pathways rather than by material composition alone. Application-oriented design should therefore coordinate material chemistry with component geometry so that carbonation remains sufficiently uniform while the desired thermal, structural, or sensing function is retained.

5.6 Performance-Oriented Design Implications

Taken together, the preceding performance results indicate that there is no single optimum γ-C_2S formulation. The dominant design variable depends on the intended function and component geometry. For precast products dominated by compressive loading, particle packing, moisture state, and internal CO_2 accessibility should be coordinated to obtain a dense but uniformly carbonated matrix. Where flexural strength or crack resistance is critical, greater emphasis should be placed on $CaCO_3$ morphology and interfacial continuity, using strategies such as aragonite bridging, Mg-calcite regulation, or organic-assisted nucleation [42,63,64]. For thicker or geometrically complex components, transport becomes the primary design constraint, and internal carbon sources, internal curing, or engineered transport pathways can be used to reduce surface-to-core reaction gradients [14,67,86]. Performance-oriented design should therefore match reaction control and product architecture to the targeted service function rather than maximize carbonation degree or strength in isolation.

Engineering translation further requires comparable testing protocols and long-term service validation.

Current studies differ substantially in specimen dimensions, forming pressure, initial moisture state, and carbonation regime, which complicates direct comparison of reported strength and CO_2 uptake. At minimum, future studies should consistently report specimen geometry, compaction conditions, moisture state, CO_2 concentration and pressure, curing duration, carbonation degree or CO_2 uptake, pore structure, and the corresponding mechanical or dimensional response. Long-term validation should additionally address chloride and sulfate exposure, freeze–thaw and wetting–drying cycles, elevated temperatures, reinforcement corrosion, and the stability of internally introduced carbonates or modifiers. Establishing these links among processing, reaction uniformity, performance, and exposure conditions is essential for translating γ-C_2S from optimized laboratory specimens to reliable engineered products.

6. Applications and Scale-Up

The engineering translation of γ-C_2S-based binders requires moving beyond material reactivity toward coordinated control of product design and manufacturing. Because γ-C_2S relies primarily on carbonation for hardening, its performance is governed not only by material composition but also by component geometry, forming conditions, moisture state, CO_2 delivery, and curing configuration. Scale-up therefore requires these factors to be integrated with product quality, durability, carbon accounting, and economic feasibility.

Direct engineering evidence for γ-C_2S is still less mature than its laboratory-scale mechanistic understanding. This section therefore evaluates its application potential together with the processing and scale-up requirements needed to translate carbonation hardening from controlled specimens to reliable engineered products.

6.1 Precast Concrete Products and Pavement Components

Precast nonstructural products provide a practical entry

point for γ-C_2S carbonation technology because component geometry, moisture condition, compaction, and CO_2 delivery can be controlled within a centralized manufacturing process. Paving blocks, curbs, revetment units, and small panels are particularly attractive because their relatively short diffusion paths and high surface-area-to-volume ratios favor more uniform carbonation. The CO_2-SUICOM system provides an early engineering demonstration of γ-C_2S-containing binders in precast concrete [87], while recent assessments of commercial CO_2-utilization technologies similarly identify small precast elements as among the most deployable product forms [5].

Recent studies on carbonation-cured paving blocks further support this manufacturing route. Vibro-compacted precast blocks with dimensions of 200 × 100 × 60 mm showed approximately 30% higher compressive strength and 60% higher splitting tensile strength after CO_2 curing, together with a reduction in abrasion mass loss from 8.2% to 5.6% [88]. A subsequent study using the same standardized paving-block geometry reported up to 34% higher compressive strength and approximately 50% lower abrasion loss, while the carbon footprint was reduced by 49% relative to Portland-cement block counterparts [89]. These results support the compatibility of carbonation curing with standardized pavement-product manufacturing, although direct field validation of γ-C_2S-based products under traffic loading, abrasion, salt scaling, freeze–thaw cycling, and long-term outdoor exposure remains necessary.

6.2 Functional and High-Value Applications

High-value functional products provide a promising early application route for γ-C_2S because they require relatively small material volumes and benefit from short carbonation paths. Carbonated γ-C_2S has been used as a protective shell for passive wireless digital aggregates, reaching approximately 95 MPa after 24 h while maintaining signal transmission [90]. Similarly, a styrene-acrylic-modified γ-C_2S coating achieved a bond strength of 4.21 MPa and formed a dense carbonate–silica-rich protective layer [91]. These applications suggest that thin, high-value components may be more readily commercialized than bulk structural products, although long-term performance under aging, moisture cycling, ultraviolet exposure, and substrate deformation remains to be validated.

6.3 Raw Materials, Mixture Design, and Forming

When γ-C_2S is transferred from controlled laboratory specimens to practical components, the dominant limitation progressively shifts from intrinsic phase reactivity to reaction–transport coupling. Increasing component size introduces longer CO_2 diffusion paths, spatial moisture gradients, and greater sensitivity to compaction and gas-flow distribution. Consequently, favorable clinker chemistry can only be translated into uniform performance when phase assemblage, forming conditions, and internal transport are designed together. Industrial feedstocks further introduce secondary phases and compositional variability, so carbonation performance cannot be inferred from γ-C_2S content alone. Recent multiphase-clinker studies show that C_2AS, amorphous phases, and residual γ-C_2S can alter both carbonation reactivity and load-bearing structure [7] . Residue-derived systems such as γ-C_2S–red mud provide additional resource benefits but require control of composition and environmental safety [92]. Industrial specifications should therefore consider overall phase assemblage, fineness, free oxides, and feedstock stability.

Forming should balance moisture availability with gas-accessible porosity. A recent γ-C_2S study reported carbonation degrees of ⩾ 45% at initial void fractions of approximately 18–28% and water volume fractions of 22–27% [23], demonstrating that water content and particle packing should be optimized together. Excessive water or compaction restricts CO_2 transport, whereas excessive drying limits dissolution and ionic transport; semi-dry forming is therefore preferable when moisture and pore accessibility are jointly controlled.

6.4 Scale-Up of Carbonation Curing

Scaling up carbonation curing shifts the main challenge from accelerating reaction kinetics to maintaining uniform CO_2 access across larger products and production batches. This size effect has been quantified at pilot scale: increasing specimen thickness from 0.5 to 4 in. reduced CO_2 uptake from 26.6% to 4.3% of cement mass, accompanied by the development of a highly carbonated surface and a nearly non-carbonated core [93]. These results show that scale-up cannot be achieved simply by extending curing time or increasing pressure; gas distribution, product geometry, moisture redistribution, and heat accumulation must be controlled together.

Recent process-scale studies further show that improved gas management can partly compensate for transport limitations. Cyclic closed-circulation flue-gas curing at ambient pressure achieved 4.86% CO_2 uptake within 48 h, close to the 5.19% obtained under high-pressure curing [94], while commercial cement-kiln exhaust-gas curing produced concrete bricks with 18 MPa compressive strength and 163.45 g CO_2 sequestration per brick [95]. Industrial scale-up should therefore be evaluated by reaction uniformity, gas-utilization efficiency, batch reproducibility, and verified carbon uptake rather than pressure or peak strength alone. The principal scale-up constraints and corresponding control parameters are summarized in Table 3.

Among these barriers, reaction–transport uniformity and process control appear to be the most immediate constraints on scale-up. Material synthesis is energy intensive, but its burden can partly be offset by industrial feedstocks and the self-pulverization of γ-C_2S, whereas nonuniform gas delivery directly limits how laboratory reactivity is translated into product-scale performance. The priority for industrialization is therefore to achieve reproducible control of CO_2 distribution, moisture state, heat evolution, and batch uniformity, while simultaneously reducing the energy demand of clinker production and carbonation curing.

Table 3. Key scale-up constraints and recommended controls for carbonation-cured γ-C_2S product

Scale-up stage	Governing constraint	Recommended control or verification	References
Feedstock and forming	Variability in phase assemblage and imbalance between moisture availability and gas-accessible porosity	QXRD/XRF, free CaO/MgO, fineness, forming density, void fraction, and water volume fraction	[6,7,23]
Carbonation curing	Increasing diffusion distance, nonuniform gas flow, and coupled heat–moisture gradients	Inlet/outlet CO_2 concentration, gas-flow rate, temperature/RH distribution, product spacing, and curing time	[93,94]
Product uniformity and quality	Surface-to-core reaction gradients and incomplete internal carbonation	Carbonation/phase profiles, spatial strength variation, dimensional stability, and product-level performance	[95]
Carbon accounting	Heterogeneous sampling, analytical interference, and inconsistency between gross uptake and lifecycle benefit	Representative sampling, TG/combustion analysis, blank correction, gas mass balance, consistent functional units and system boundaries	[96,97]
Engineering deployment	Batch reproducibility, gas utilization, production energy, and field-performance uncertainty	Batch variability, gas-utilization efficiency, energy demand, process monitoring, and long-term field validation	[5]

6.5 Product Quality, Durability, and Standardization

Engineering acceptance of γ-C_2S products should extend beyond short-term strength because carbonation-induced densification does not translate uniformly into long-term durability. In a recent carbonation-cured precast system, 24 h of CO_2 curing reduced the chloride migration coefficient from 17.5 ± 1.6 to 0.78 ± 0.15 × 10^{-12} m^2/s, a reduction of approximately 95%, while the material also remained within specification limits after 100 freeze–thaw cycles [98]. However, such improvements are strongly mixture-dependent. In in-situ carbonated concrete, the chloride migration coefficient changed from 39.27 to 34.15 × 10^{-12} m^2/s in one mixture, but from 25.99 to 26.18 × 10^{-12} m^2/s in another, corresponding to a 13.0% reduction and a 0.76% increase, respectively; carbonation also reduced 28-day strength in some mixtures [99]. These contrasting responses indicate that carbonation itself should not be treated as a durability guarantee. Product acceptance should instead verify whether the resulting pore structure and reaction uniformity deliver the durability required for the intended exposure condition.

Reliable product qualification also requires comparable CO_2-uptake measurements. A recent inter-method comparison of five analytical approaches showed that, after appropriate sample drying, CO_2 release by heating to ⩾ 980° C or HCl treatment combined with NDIR or coulometric detection achieved measurement variances within ±5%, whereas H_3PO_4 treatment underestimated CO_2 content by as much as 12%. Thermogravimetric methods can additionally under- or overestimate uptake when H_2O and CO_2 mass-loss ranges overlap [100]. Standardization should therefore focus not only on the reporting unit, but also on representative sampling, moisture conditioning, carbonate-release procedure, analytical range, and independent verification of CO_2 uptake.

6.6 Environmental and Economic Feasibility

The environmental advantage of γ-C_2S cannot be evaluated from gross CO_2 uptake alone, because the CO_2 mineralized during curing must be balanced against emissions associated with raw-material preparation, clinker firing, grinding, CO_2 capture and conditioning, curing energy, and transportation. This distinction is particularly important when γ-C_2S is compared with OPC and other low-carbon binders, which reduce emissions through different pathways. As summarized in Table 4, recent comparative assessments indicate that LC^3 and alkali-activated binders can reduce carbon impacts by approximately 40% and 40–75%, respectively, relative to OPC, whereas carbonatable binders as a broader class have been estimated to provide reductions of approximately 37% [2]. γ-C_2S provides an additional mineralization pathway, with experimental CO_2 uptake reaching approximately 230 kg CO_2 per tonne of binder. However, this gross uptake should not be interpreted directly as an equivalent reduction in lifecycle emissions.

Table 4. Representative environmental and economic benchmarks for γ-C_2S and selected low-carbon binder and carbonation routes

Binder / process	Representative carbon metric	Representative energy or economic metric
OPC [2]	0.820 kg CO_2-eq/kg cement	Embodied energy ≈ 4.72 MJ/kg cement
LC^3 [2]	40% lower carbon impact than OPC	Generally compatible with conventional cement production; cost advantage is feedstock- and location-dependent
Alkali-activated materials [2]	40–75% lower carbon impact than OPC	Activator production can contribute substantially to energy use and cost
Carbonatable binders [2]	37% lower carbon impact than OPC	Additional CO_2 supply and curing infrastructure required
γ-C_2S [6,29]	Gross CO_2 uptake up to ≈ 230 kg CO_2/t binder	Self-pulverization can reduce clinker-grinding electricity by ≈ 30–40% relative to conventional cement production
Industrial mineralization-curing demonstration [101]	≈ 182 kg CO_2-eq/m^3 lower GWP than autoclaved curing; CO_2 conversion >98%	Economic benefit ≈ 35 USD/t-CO_2

Note: The reported values originate from studies with different functional units, system boundaries, electricity mixes, raw-material allocation methods, and carbonation configurations. They are therefore intended as representative benchmarks rather than directly interchangeable values. Process-level data from broader carbonation-curing systems are included because γ-C_2S-specific industrial LCA, curing-energy, and production-cost datasets remain limited.

The economic feasibility of γ-C_2S remains strongly process- and supply-chain-dependent. A recent techno-economic comparison of CO_2 mineralization routes found that only three of six scenarios were economically viable below a carbon price of 100 € /t-CO_2 [102], highlighting the sensitivity of mineralization economics to feedstock supply, CO_2 sourcing, energy demand, and transport. A γ-C_2S-specific lifecycle and cost inventory is still lacking; future assessments should therefore adopt consistent functional units and transparent system boundaries while distinguishing gross CO_2 uptake from avoided emissions and net lifecycle reduction.

7. Conclusions and Prospects

This review has examined γ-C_2S-based binders across the production–carbonation–structure–performance–application chain. The available evidence indicates that the engineering potential of γ-C_2S cannot be judged by carbonation degree or CO_2 uptake alone, but depends on how phase assemblage, reaction–transport coupling, carbonation-product organization, and manufacturing conditions collectively translate mineralization into reliable performance. The main conclusions and prospects are summarized as follows:

(1) Carbonation-induced hardening of γ-C_2S is fundamentally a process of structural reorganization rather than simple CO_2 uptake. Water-assisted decalcification releases Ca^{2+} from the silicate lattice, followed by $CaCO_3$ precipitation and progressive polymerization of the residual silica-rich phase. Mechanical performance therefore depends not only on reaction extent but also on carbonate polymorphism, silica-network connectivity, product distribution, and interfacial bonding. Excessive surface precipitation may simultaneously strengthen the outer matrix and restrict subsequent transport, explaining why a higher carbonation degree does not necessarily produce higher strength. Future mechanistic studies should therefore move beyond endpoint phase identification toward spatially and temporally resolved descriptions of reaction fronts and product evolution. Recent advances in X-ray attenuation and diffraction computed tomography enable three-dimensional mapping of carbonation-induced phase and pore redistribution [103], while pore-structure-informed multiphysics models provide a route to couple CO_2 and moisture transport, heat transfer, reaction kinetics, and evolving pore structure [104] .

(2) Material design should shift from maximizing

γ-C_2S purity toward controlling the overall reactive phase assemblage. High-purity γ-C_2S remains valuable for identifying intrinsic reaction pathways, but industrial clinkers inevitably contain secondary crystalline and amorphous phases that alter dissolution, carbonate nucleation, moisture retention, and interparticle bonding. A lower γ-C_2S fraction can therefore remain mechanically effective when the accompanying phases organize carbonation and load transfer favorably. The key industrial question is consequently not how to reproduce laboratory-grade purity, but how much compositional variability can be tolerated without losing reaction uniformity, dimensional stability, or environmental safety. Future work should establish acceptable windows for phase assemblage, free oxides, fineness, trace elements, and residue-derived constituents. This shift is consistent with recent assessments of carbonatable industrial wastes, which identify feedstock variability, phase composition, environmental compatibility, and industrial reproducibility as central requirements for deployment [105].

(3) The most immediate scale-up barrier is the loss of reaction–transport uniformity as product size and production complexity increase. Laboratory reactivity can only be translated into engineering performance when sufficient interfacial moisture for dissolution and ionic transport is maintained together with connected gas-accessible pathways. As diffusion distances increase, surface carbonation, pore closure, moisture redistribution, and reaction heat progressively generate surface-to-core heterogeneity. Scale-up should therefore focus less on maximizing nominal CO_2 pressure and more on controlling product geometry, gas circulation, spacing, moisture state, temperature, and batch-to-batch reproducibility. Curing-chamber design and process monitoring should be developed together, with spatial carbonation profiles used to verify product uniformity. At the same time, high-temperature clinker production and CO_2 conditioning remain important system-level energy burdens; process intensification is only meaningful when improved reaction efficiency outweighs the additional energy required to achieve it.

(4) Thin, standardized, nonreinforced precast products currently provide the most credible route toward near-term application. Paving blocks, curbs, revetment units, small panels, coatings, and other thin functional components combine short CO_2 diffusion paths with centralized forming and curing, making carbonation easier to control than in thick structural members. High-value applications such as coatings and digital aggregates may provide an additional entry route because they exploit carbonation-induced densification while requiring comparatively small material volumes. In contrast, widespread use in reinforced structural concrete remains premature because extensive carbonation lowers pore-solution alkalinity, while long diffusion paths increase the risk of incomplete internal reaction. Product qualification should therefore move from short-term strength toward exposure-specific performance, including transport resistance, dimensional stability, freeze–thaw and salt resistance, interfacial durability, and reinforcement compatibility. More broadly, recent durability research on low-carbon binders reinforces the need to link binder chemistry and pore evolution to specific degradation mechanisms rather than assuming that densification alone ensures durability [106].

(5) The environmental value of γ-C_2S must ultimately be demonstrated at the manufacturing-system level rather than inferred from gross CO_2 uptake. Mineralized CO_2 should be balanced against emissions associated with raw-material preparation, firing, grinding, CO_2 capture and conditioning, curing energy, transportation, and product service life. Likewise, economic feasibility depends on the local coupling among feedstock supply, CO_2 source, production rate, curing infrastructure, and market value. Future demonstrations should therefore report spatial carbonation uniformity, production energy, gas-utilization efficiency, durability, cost, and verified carbon benefit within consistent functional units and transparent system boundaries. Stored CO_2, avoided emissions, and net lifecycle reduction should be reported separately. Recent scale-up assessments similarly indicate that the transition from carbonation chemistry to commercial deployment increasingly depends on integrating process control, carbon quantification, techno-economics, standards, and implementation pathways [107]. For γ-C_2S, progress should therefore proceed from laboratory validation to pilot manufacturing, field monitoring, and lifecycle verification before expansion toward larger or reinforced structural applications.

Declaration of competing interest

The authors declare that they have no known competing financial interests or personal relationships that could have appeared to influence the work reported in this paper.

Acknowledgements

The authors would like to acknowledge the financial support from the National Key Research and Development Program of China (Grant No.2023YFE0121400), Science and Technology Commission of Shanghai Municipality (Grant No. 23DZ1202103) and Key Research and Development Program of Shanxi Province (Grant No. 202402090301029).

References

[1] R. Chaudhury, U. Sharma, P.C. Thapliyal, L.P. Singh, Low-CO_2 emission strategies to achieve net zero target in cement sector, J. Clean. Prod. 417 (2023) 137466.

[2] M.R. Ahmad, A. Fernàndez-Jimenez, B. Chen, Z. Leng, J.-G. Dai, Low-carbon cementitious materials: Scale-up potential, environmental impact and barriers, Constr. Build. Mater. 455 (2024) 139087.

[3] X. Hu, P. He, C. Shi, Carbonate binders: historic developments and perspectives, Cem. Concr. Res. 175 (2024) 107352.

[4] Z. Liu, C. Lv, F. Wang, S. Hu, Recent advances in carbonatable binders, Cem. Concr. Res. 173 (2023) 107286.

[5] D. Zhang, CO_2 utilization for concrete production:

Commercial deployment and pathways to net-zero emissions, Science of The Total Environment 931 (2024) 172753.

[6] H. Huang, C. Lv, Z. Liu, F. Wang, S. Hu, Development of industrial-grade γ-C_2S binder from limestone and sandstone: preparation, properties, and microstructure, Constr. Build. Mater. 411 (2024) 134486.

[7] C. Lv, Z. Liu, F. Wang, S. Hu, Understanding the role of different phases in γ-C_2S based carbonatable clinkers, Cem. Concr. Res. 185 (2024) 107642.

[8] S. Li, J. Xue, G. Li, L. Zhang, R. Zhao, S. Liu, X. Guan, New insights into the carbonation disparities and underlying mechanisms of β-C_2S and γ-C_2S: An experimental and theoretical investigation, J. Clean. Prod. 543 (2026) 147596.

[9] Y. Gao, Y. Tao, G. Li, P. Shen, R.J.-M. Pellenq, C.S. Poon, Moisture-driven carbonation kinetics for ultrafast CO_2 mineralization, Proceedings of the National Academy of Sciences 122 (2025) e2418239121.

[10] Y. Tan, Z. Liu, F. Wang, Effect of temperature on the carbonation behavior of γ-C_2S compacts, Cem. Concr. Compos. 133 (2022) 104652.

[11] J. Másilko, E. Bartoníčková, R. Novotný, J. Švec, M. Sedlačík, V. Cába, D. Markusík, J. Koplík, L. Kalina, M. Březina, Calorimetric study of gamma dicalcium silicate during the accelerated carbonation process, J. Therm. Anal. Calorim. 151 (2026) 2905–2914.

[12] M. Lei, Z. Liu, F. Wang, S. Hu, Understanding the uneven phase distribution and multi-step reaction mechanism of carbonated γ-C_2S-based foam concrete, Cem. Concr. Compos. 154 (2024) 105803.

[13] X. Wang, H. Luo, F. Zou, J. Cai, Y. Yu, J. Fu, High-performance CO_2 sequestration solid materials consist of β-C_2S and γ-C_2S binary clinkers synthesized from carbide slag and sandstone: sintering, carbonation, and microstructure, ACS Sustain. Chem. Eng. 12 (2024) 6840–6855.

[14] K. Ye, L. Yang, J. Zeng, J. Tian, F. Zeng, G. Ye, Y. Mu, Enhancing the strength of carbonated γ-dicalcium silicate by internal carbonation curing, Constr. Build. Mater. 469 (2025) 140512.

[15] J.S. Ndzila, Z. Yang, Carbonation properties of ion-doped non-hydraulic calcium silicate binders: A review, Journal of Building Engineering 105 (2025) 112427.

[16] K. Yang, B. Yuan, B. Li, J. Li, W. Chen, Iron corrosion behavior in carbonated γ-C_2S binders: Impact of CO_2 exposure on corrosion product, Journal of Building Engineering 111 (2025) 113323.

[17] X. Wang, M.-Z. Guo, T.-C. Ling, Review on CO_2 curing of non-hydraulic calcium silicates cements: mechanism, carbonation and performance, Cem. Concr. Compos. 133 (2022) 104641.

[18] X. Zhang, H. Na, P. Liu, Y. Wang, J. Li, Q. Meng, G. Li, A Novel "Two-Step" γ → α ′ L → β phase transformation method for dicalcium silicate in AOD slag for improving hydration activity, Metallurgical and Materials Transactions B 54 (2023) 712–733.

[19] C. Gregson, R.A. Brooker, S.C. Kohn, O.T. Lord, Thermodynamic and kinetic controls on phase stability and incorporation of water in larnite (β-Ca_2SiO_4): Implications for calcium silicate inclusions in diamonds, Contributions to Mineralogy and Petrology 179 (2024) 82.

[20] N. Li, D. Ai, T. He, Z. Liu, J. Zeng, J. Yang, X. Zhi, F. Jia, J. Ye, X. He, Probing the early stages of hydration in dicalcium silicates at electronic level, Journal of the American Ceramic Society 108 (2025) e20550.

[21] N. Li, J. Peng, X. Zhi, J. Ye, F. Jia, W. Chen, F. Wang, The synergistic effect of water and lattice oxygen on CO_2 mineralization in γ - dicalcium silicate, Journal of the American Ceramic Society 108 (2025) e70026.

[22] S. Wang, F. Zou, H. Luo, An all solid waste CO_2 sequestration material consist of multiple calcium silicate clinkers by carbide slag, copper tailing and red mud: Clinker crystal transformation and carbonation hardening properties, Constr. Build. Mater. 450 (2024) 138534.

[23] Z. Zhang, K. Zheng, L. Chen, Y. Yang, T. Xie, Q. Yuan, Q. Cao, Optimization of initial porosity and influence on carbonation behavior of γ-dicalcium silicate, Constr. Build. Mater. 470 (2025) 140658.

[24] H. Liu, C. Lv, S. Zhao, Z. Liu, Y. Zheng, F. Wang, Ion-doped γ-C_2S: clinker characteristics, carbonation products, and carbonation properties, Constr. Build. Mater. 438 (2024) 137033.

[25] C. Duée, C. Bourgel, E. Véron, M. Allix, F. Fayon, F. Bodénan, J. Poirier, Phosphorus speciation in dicalcium silicate phases: Application to the basic oxygen furnace (BOF) slag, Cem. Concr. Res. 73 (2015) 207–214.

[26] X. Zhang, G. Li, H. Na, P. Liu, J. Li, Q. Meng, Y. Duan, Y. Zhang, The role of P_2O_5 on the stability of β-C_2S in AOD slag based on the improvement of hydration activity, J. Alloys Compd. 968 (2023) 172221.

[27] L. Zhu, M. Shi, H. Lyu, Y. Liu, S. Zhang, C.S. Poon, Innovative two-step synthesis design approach in developing vanadium incorporated low-carbon binder system, Cem. Concr. Res. 197 (2025) 107977.

[28] Y. Tao, Y. Mu, W. Zhang, F. Wang, Screening Out Reactivity-Promoting Candidates for γ-Ca_2SiO_4 Carbonation by First-Principles Calculations, Front. Mater. Volume 7-2020 (2020). https://www.frontiersin.org/journals/materials/articles/10.3389/fmats.2020.00299.

[29] X. Guan, S. Liu, C. Feng, M. Qiu, The hardening behavior of γ-C_2S binder using accelerated carbonation, Constr. Build. Mater. 114 (2016) 204–207.

[30] X. Du, J. Chang, L. Lin, X. Peng, H. Han, Y. Bai, Performance differences and mechanism of carbonation-hardened compacts produced with different C_2S polymorphs: A new perspective of carbonatable binder, Cem. Concr. Compos. 163 (2025) 106216.

[31] S. Zhao, Z. Liu, F. Wang, S. Hu, Elucidating factors on the strength of carbonated compacts: Insights from the carbonation of γ-C_2S, β-C_2S and C_3S, Cem. Concr. Compos. 155 (2025) 105806.

[32] J. Yue, X. Zhang, Z. Li, H. Zou, Y. Wang, W. Chen, X. He, N. Li, Oxygen Vacancy Mediated Carbonation of γ - C_2S: Combined Ab Initio Calculations and OPES Enhanced Sampling Insights, Journal of the American Ceramic Society 109 (2026) e70723.

[33] H. Zou, Z. Zhang, Z. Li, J. Yue, B. Liu, W. Chen, N. Li, Unlocking Deep Carbonation in γ - C_2S by Iron Dopant: Suppressing Surface Reaction to Promote Dissolution–Precipitation, Journal of the American Ceramic Society 109 (2026) e70679.

[34] W. Ashraf, J. Olek, Carbonation activated binders from pure calcium silicates: Reaction kinetics and performance controlling factors, Cem. Concr. Compos. 93 (2018) 85–98.

[35] Y. Mu, Z. Liu, F. Wang, Comparative study on the carbonation-activated calcium silicates as sustainable binders: reactivity, mechanical performance, and

microstructure, ACS Sustain. Chem. Eng. (2019).
[36] Z.X. Chen, N.T. Zhang, S.H. Chu, Role of alkalinity in CO_2 sequestration of γ-belite, Constr. Build. Mater. 432 (2024) 136508.
[37] H. Zhou, P. Liu, F. Wang, C. Hu, Carbonation of Dicalcium Silicate Enhanced by Ammonia Bicarbonate and Its Mechanism, Journal of Wuhan University of Technology-Mater. Sci. Ed. 39 (2024) 69–74.
[38] G. Li, S. Liu, X. Hu, J. Zhu, X. Guan, C. Shi, Effect of pH environment on carbonation properties of γ-C_2S, Constr. Build. Mater. 461 (2025) 139888.
[39] X. Fu, A. Guerini, D. Zampini, A.F. Rotta Loria, Storing CO_2 while strengthening concrete by carbonating its cement in suspension, Commun. Mater. 5 (2024) 109.
[40] J. Chang, Y. Fang, X. Shang, The role of β-C_2S and γ-C_2S in carbon capture and strength development, Mater. Struct. 49 (2016) 4417–4424.
[41] Z.X. Chen, S.H. Chu, S. Ishak, H.S. Lee, Q.X. Zhao, D.Y. Yoo, Roles of particle packing and water coating thickness in carbonation and strength of γ-dicalcium silicate-based low carbon materials, J. Clean. Prod. 358 (2022) 131735.
[42] L. Yu, S. Wang, X. Kong, B. Lu, J. Sun, J. Ma, R. Jiang, Z. Zhang, G. Hou, Influence of mass content of in-situ formed aragonite on the mechanical strength and pore structure of γ-C_2S carbonation, Constr. Build. Mater. 456 (2024) 139373.
[43] R. Pengjie, T. Pei, C. Wei, Regulating mechanism of ammonium salt on mechanical and microstructural properties of γ-C_2S binder via CO_2 curing, Constr. Build. Mater. 495 (2025) 143637.
[44] R.W.M. Jensen, J. Skibsted, Aqueous Carbonation of Calcium Silicates With Different Ca/Si Ratios Studied by Solid‐State NMR Spectroscopy, Magnetic Resonance in Chemistry 63 (2025) 476–494.
[45] J. Qi, L. Yu, G. Wang, Z. Hu, H. Shen, B. Lu, R. Jiang, W. Xu, R. Shao, G. Hou, Which one among the in-situ formed calcite, aragonite or vaterite is more beneficial to the carbonated γ-C_2S performance: Mechanical strength, pore structure, Constr. Build. Mater. 513 (2026) 145420.
[46] A. Smigelskyte, R. Siauciunas, H. Hilbig, M. Decker, L. Urbonas, G. Skripkiunas, Carbonated rankinite binder: effect of curing parameters on microstructure, strength development and durability performance, Sci. Rep. 10 (2020) 14462.
[47] K. Luo, W. Zhang, J. Ye, J. Li, Z. Lu, X. Ren, Mechanism of interaction between hydration–carbonation of C_2S, Constr. Build. Mater. 412 (2024) 134891. https://doi.org/10.1016/j.conbuildmat.2024.134891.
[48] Y. Yi, W. Ma, A. Sidike, Z. Ma, M. Fang, Y. Lin, S. Bai, Y. Chen, Synergistic effect of hydration and carbonation of ladle furnace aslag on cementitious substances, Sci. Rep. 12 (2022) 14526. https://doi.org/10.1038/s41598-022-18215-7.
[49] C. Zhang, X. Guan, J. Zhu, S. Liu, R. Zhao, Investigation of curing behavior of γ-C_2S and MgO under varying CO_2 concentrations, Constr. Build. Mater. 455 (2024) 139176. https://doi.org/10.1016/j.conbuildmat.2024.139176.
[50] S. Zhao, Z. Liu, F. Wang, S. Hu, C. Liu, Effect of Extended Carbonation Curing on the Properties of γ-C_2S Compacts and Its Implications on the Multi-Step Reaction Mechanism, ACS Sustain. Chem. Eng. 9 (2021). https://doi.org/10.1021/acssuschemeng.1c00200.
[51] T. Chen, P. Xu, X. Gao, T. Wang, L. Qin, New sights in early carbonation of calcium silicates: Performance, mechanism and nanostructure, Constr. Build. Mater. 314 (2022) 125622. https://doi.org/10.1016/j.conbuildmat.2021.125622.
[52] B. Lu, S. Drissi, J. Liu, X. Hu, B. Song, C. Shi, Effect of temperature on CO_2 curing, compressive strength and microstructure of cement paste, Cem. Concr. Res. 157 (2022) 106827. https://doi.org/10.1016/j.cemconres.2022.106827.
[53] X. Zhang, Z. Liu, F. Wang, Effect of coral powder on the carbonation behavior of γ-C_2S, Constr. Build. Mater. 347 (2022) 128251. https://doi.org/10.1016/j.conbuildmat.2022.128251.
[54] A. Gineika, R. Siauciunas, K. Baltakys, Synthesis of wollastonite from AlF_3-rich silica gel and its hardening in the CO_2 atmosphere, Sci. Rep. 9 (2019) 18063. https://doi.org/10.1038/s41598-019-54219-6.
[55] T. Jiang, K. Cui, J. Chang, Development of low-carbon cement: Carbonation of compounded C_2S by β-C_2S and γ-C_2S, Cem. Concr. Compos. 139 (2023) 105071. https://doi.org/10.1016/j.cemconcomp.2023.105071.
[56] A. Peys, N. Pires Martins, F. Prado Araujo, P. Nielsen, Akermanitic clinker unlocks the potential of Mg-silicates for carbonation cured construction materials, Front. Mater. 12 (2025) 1570367.
[57] Y. Mu, Z. Liu, F. Wang, X. Huang, Effect of barium doping on carbonation behavior of γ-C_2S, Journal of CO_2 Utilization 27 (2018) 405–413. https://doi.org/10.1016/j.jcou.2018.08.018.
[58] S. Zhao, Z. Liu, Y. Mu, F. Wang, Y. He, Effect of chitosan on the carbonation behavior of γ-C_2S, Cem. Concr. Compos. 111 (2020) 103637. https://doi.org/10.1016/j.cemconcomp.2020.103637.
[59] S. Zhao, Z. Liu, F. Wang, Carbonation reactivity enhancement of γ-C_2S through biomineralization, Journal of CO_2 Utilization 39 (2020) 101183.
[60] L. Yu, B. Lu, J. Sun, R. Jiang, Z. Liu, Z. Zhang, H.M. Naguib, G. Hou, A novel approach to accelerate the carbonation of γ-C_2S under atmospheric pressure: Increasing CO_2 dissolution and promoting calcium ion leaching via triethanolamine, Constr. Build. Mater. 450 (2024) 138719.
[61] K. Ye, G. Huang, Y. Zhao, Q. Hou, J. Chen, J. Tian, G. Ye, Y. Mu, Effect of CAC addition and pre-drying on the mechanical property of carbonated C_2S (γ) mortar, Constr. Build. Mater. 456 (2024) 139293.
[62] R.M. Ghantous, M.N. Goodwin, M.K. Moradllo, S. Quinn, V. Aktan, B.O. Isgor, S. Reese, J.W. Weiss, Examining Carbonation of calcium silicate-based cements in real time using neutron radiography, Materials Journal 120 (2023).
[63] Y. Liang, Y. Liu, Z. Liu, F. Wang, S. Hu, Enhancement of flexural strength of γ-C_2S carbonated compacts through in situ synthesis of Mg-calcite, Compos. B Eng. 297 (2025) 112331.
[64] M.I. Haque, I.B. Borno, W. Ashraf, Enhancing the properties of carbonation cured gamma dicalcium silicates (γ-C_2S) using biomimetic molecules, J. Sustain. Cem. Based. Mater. 13 (2024) 690–705.
[65] L. Yu, J. Qi, Y. Wang, B. Lu, J. Sun, J. Ma, R. Jiang, Z. Zhang, G. Hou, The distinct impacts of in-situ formed calcite and vaterite on the mechanical strength and microstructure of carbonated γ-C_2S, Constr. Build. Mater. 487 (2025) 142148.
[66] Z. Zhang, K. Zheng, L. Chen, Q. Yuan, Enhancing carbonation-activated γ-C_2S compacts through Na_2CO_3 post-curing: Alkalinity and mechanical properties improvement, Journal of Building Engineering 103 (2025) 112136.
[67] A. Bersisa, K.-Y. Moon, G.M. Kim, J.-S. Cho, S. Park, Internal carbonation of calcium silicate cement incorporated with Na_2CO_3 and $NaHCO_3$, Constr. Build. Mater. 462 (2025) 139732.

[68] S. Cho, H. Suh, G. Kim, J. Liu, P. Li, S. Bae, Microstructural phase evolution and strength development of low-lime calcium silicate cement (CSC) paste incorporating ordinary Portland cement under an accelerated carbonation curing environment, Constr. Build. Mater. 411 (2024) 134248.
[69] A. Bersisa, K.-Y. Moon, G.M. Kim, J.-S. Cho, S. Park, Influence of hydraulic cement substitutes on carbonation of calcium silicate cement, Constr. Build. Mater. 473 (2025) 140800.
[70] H. Al Kindi, H.A. Abdel-Gawwad, M.S. Meddah, K. Al Jabri, Y. Mohamedzein, An overview of the critical influential parameters on the performance of limestone calcined clay cement paste, mortar, and concrete, Constr. Build. Mater. 444 (2024) 137615.
[71] C. Xue, V. Sirivivatnanon, A. Nezhad, Q. Zhao, Comparisons of alkali-activated binder concrete (ABC) with OPC concrete-A review, Cem. Concr. Compos. 135 (2023) 104851.
[72] Z. Zhang, K. Zheng, H. Song, L. Chen, Q. Yuan, Q. Cao, Enhancing the Mechanism of Inert Fillers on Carbonation Properties of γ-Calcium Silicate Compacts, ACS Sustain. Chem. Eng. 13 (2025) 17103–17118.
[73] A. Bersisa, K.-Y. Moon, G.M. Kim, J.-S. Cho, S. Park, Microstructural characterization of CO_2-cured calcium silicate cement, Developments in the Built Environment 19 (2024) 100518.
[74] A. Leemann, F. Winnefeld, B. Münch, F. Läng, Carbonated wollastonite–An effective supplementary cementitious material?, J. Microsc. 286 (2022) 120–125.
[75] K. Huang, M. Lei, Z. Liu, H. Huang, F. Wang, S. Hu, Carbon-absorbing inorganic coating with ultrahigh bonding strength for concrete: bonding, durability performances, and the underlying mechanisms, ACS Sustain. Chem. Eng. 12 (2024) 8188–8202.
[76] Y. Farnam, C. Villani, T. Washington, M. Spence, J. Jain, W.J. Weiss, Performance of carbonated calcium silicate based cement pastes and mortars exposed to NaCl and $MgCl_2$ deicing salt, Constr. Build. Mater. 111 (2016) 63–71.
[77] A. Bersisa, S. Kim, N. Kim, J. Seo, K.-Y. Moon, G.M. Kim, J.-S. Cho, S. Park, Microstructural and durability assessment of carbonated calcium silicate cement under sulfate attack, Journal of Building Engineering (2025) 114269.
[78] Y. Zhou, C. Zhang, Q. Zhou, M. Guo, R. Hu, Unveiling the role of LC^3 in chloride penetration resistance of chloride contaminated mortar, Constr. Build. Mater. 458 (2025) 139658.
[79] H.S. Gökçe, Durability of slag-based alkali-activated materials: A critical review, Journal of the Australian Ceramic Society 60 (2024) 885–903.
[80] Y. Mu, Z. Liu, F. Wang, Study on heat resistance of carbonated γ-C_2S binder: Strength, phase and microstructure evolution, Constr. Build. Mater. 329 (2022) 127049.
[81] Z. Yu, X. Wang, X. Xian, T.-C. Ling, Thermal behavior of carbonated γ-C_2S compacts subjected to high temperature: mechanical properties and phase evolution, Constr. Build. Mater. 451 (2024) 138799.
[82] X. Zhou, Y. Mu, Z. Liu, F. Wang, Fabrication and characterization of a novel carbonated 0-3 piezoelectric γ-C_2S composite, Ceram. Int. 44 (2018) 13426–13429.
[83] Z. Zhu, H. Huang, Z. Liu, F. Wang, Development of high-performance piezoelectric composites for concrete construction through carbonation of calcium and magnesium-based binder, Constr. Build. Mater. 449 (2024) 138359.
[84] A. Thomas, C.R. Yörük, M.C. Usta, N.-L. Pantšenko, T. Hain, M. Uibu, A. Trikkel, Developing mineral foam blocks from oil shale byproducts through accelerated carbonation, ACS Omega 10 (2025) 47051–47064.
[85] Y. Wang, Q. Xu, B. Lu, J. Sun, Z. Zhang, C. Hu, G. Hou, A novel approach for the preparation of low thermal conductivity foam concrete with γ-C_2S carbonation and aragonite-reinforced pore walls, Constr. Build. Mater. 492 (2025) 142934.
[86] N. Ralston, S. Gupta, R. Moini, 3D-printing of architected calcium silicate binders with enhanced and in-situ carbonation, Virtual Phys. Prototyp. 19 (2024) e2350768.
[87] T. Higuchi, M. Morioka, I. Yoshioka, K. Yokozeki, Development of a new ecological concrete with CO_2 emissions below zero, Constr. Build. Mater. 67 (2014) 338–343.
[88] A.M. Merino-Lechuga, G. Lamaa, R.V. Silva, J. de Brito, J.R. Jiménez, J.M. Fernández-Rodríguez, Á. González-Caro, Accelerated carbonation of alkali-activated vibro-compacted pervious concrete paving blocks, Constr. Build. Mater. 449 (2024) 138458.
[89] A.M. Merino-Lechuga, G. Lamaa, R.V. Silva, J. de Brito, J.R. Jiménez, J.M. Fernández-Rodríguez, Á. González-Caro, Technical and environmental assessment of CO_2-cured alkali-activated pervious paving blocks incorporating recycled aggregates, Constr. Build. Mater. 489 (2025) 142286.
[90] H. Ding, H. Huang, Z. Liu, F. Wang, Digital aggregate for concrete smart management and lifecycle traceability from gamma-dicalcium silicate carbonation, Constr. Build. Mater. 472 (2025) 140869.
[91] Y. Liang, P. Liu, Y. Liu, Z. Xia, C. Hu, Z. Liu, F. Wang, S. Hu, Preparation of carbon capture coating for concrete from γ-C_2S and styrene-acrylic copolymer latex, Journal of Building Engineering (2025) 113928.
[92] Y. Yang, S. Liu, L. Xu, J. Fang, W. Wang, K. Wu, Z. Yang, Feasibility of carbon dioxide uptake cementitious materials preparation by combining γ-C_2S with red mud, Constr. Build. Mater. 412 (2024) 134672.
[93] D. Zhang, B. Feng, B. Jaworska, B.R. Ellis, S. Fancy, V. Sick, V.C. Li, Pilot-scale validation of CO_2 utilization for greener and tougher infrastructure through carbonation curing of bendable concrete, J. Clean. Prod. 491 (2025) 144845.
[94] X. Xian, B. Yu, Flue gas carbonation curing under ambient pressure: A sustainable approach for precast railway concrete products, Journal of Railway Science and Technology (2026).
[95] Y. Li, J. Tian, Y. Wang, J. Liu, X. Hu, X. You, Y. Mao, C. Shi, Properties and microstructure of carbonated concrete brick through CO_2 mineralization with cement kiln exhaust gas, Constr. Build. Mater. 499 (2025) 144153.
[96] J.A. Olsson, S.A. Miller, J.D. Kneifel, A review of current practice for life cycle assessment of cement and concrete, Resour. Conserv. Recycl. 206 (2024) 107619.
[97] T. Matschei, S. Braymand, N. Garg, B. Huet, D. Jansen, R.J. Myers, B. Scruggs, E. Bernard, J. Bertola, B. Cazacliu, Test methods for CO_2 mineralization in cement-based materials: A review by RILEM TC 309-MCP, Mater. Struct. 59 (2026) 175.
[98] W. Li, H. Wang, Z. Liu, N. Li, S. Zhao, S. Hu, Steel slag accelerated carbonation curing for high-carbonation precast concrete development, Materials 17 (2024) 2968.
[99] M.N. Seifu, J.K. Adem, H.R. Khalid, G.M. Kim, S. Park, Effects of Water-to-Binder Ratios on the Workability, Durability and Strength Development of In-Situ Carbonated Concrete, Int. J. Concr. Struct. Mater. 19 (2025) 96.
[100] K. Namiki, K. Yamashita, K. Tabara, S. Noda, Comparison

and reliability assessment of CO_2 quantification methods for carbonated cementitious materials, Journal of CO_2 Utilization 97 (2025) 103140.

[101] T. Wang, Z. Yi, J. Song, C. Zhao, R. Guo, X. Gao, An industrial demonstration study on CO_2 mineralization curing for concrete, IScience 25 (2022).

[102] A. Abdelshafy, T. Strunge, D. Stephan, G. Walther, A comparative techno-economic assessment of CO_2 mineralization technologies: A case study from the construction sector, Journal of CO_2 Utilization 96 (2025) 103092.

[103] Z. Yue, Z. Su, P.P. Paul, A.T.M. Marsh, A. Macente, M. Di Michiel, J.L. Provis, P.J. Withers, S.A. Bernal, 3D crystalline phase and pore structure evolution upon CO_2 exposure in sodium sulfate-activated cement pastes, Cem. Concr. Res. 187 (2025) 107716.

[104] W. Chen, C. Chang, Y. Li, C. Xu, J. Deng, W. Li, Y. Jin, Y. Zhou, A pore-structure-informed multiphysics carbonation model enabling evaluation of durability and CO_2 sequestration potential of sustainable cementitious materials, J. Clean. Prod. 568 (2026) 148673.

[105] C. Lv, Z. Liu, F. Wang, S. Hu, Industrial solid wastes as carbonatable binders for abating CO_2 emission, Renewable and Sustainable Energy Reviews 214 (2025) 115557.

[106] A. Machner, P. Suraneni, K. De Weerdt, M.E. Krüger, W. Wilson, O.B. Isgor, Durability of concrete prepared with low-carbon binders: Perspectives and insights, Cem. Concr. Res. 206 (2026) 108273.

[107] S. Cho, N. Lee, M.O. Kim, Is CO_2 utilization in cement and concrete ready for scale-up? Mechanisms, quantification, and policy pathways, Resour. Conserv. Recycl. 232 (2026) 108983.